













Phosphorylation of the plasma membrane H⁺-ATPase AHA2 by BAK1 is required for ABA-induced stomatal closure in Arabidopsis

Dan Pei ,¹ Deping Hua ,² Jinping Deng ,¹ Zhifang Wang ,¹ Chunpeng Song ,³ Yi Wang ,¹ Yu Wang ,¹ Junsheng Qi ,¹ Hannes Kollist ,⁴ Shuhua Yang ,¹ Yan Guo ¹ and Zhizhong Gong ^{1,5,*†}

- 1 State Key Laboratory of Plant Physiology and Biochemistry, College of Biological Sciences, China Agricultural University, Beijing 100193, China
- 2 School of Life Sciences, Tianjin University, Tianjin 300072, China
- 3 Collaborative Innovation Center of Crop Stress Biology, Institute of Plant Stress Biology, Henan University, Kaifeng 475001, China
- 4 Plant Signal Research Group, Institute of Technology, University of Tartu, Tartu 50411, Estonia
- 5 School of Life Sciences, Institute of Life Science and Green Development, Hebei University, Baoding 071002, China

*Author for correspondence: gongzz@cau.edu.cn

†Senior author

Z.G. and P.D. designed research. P.D. and D.H. performed research. P.D., Z.G., J.D., Z.W., D.H., and Y.G. analyzed data, and P.D. and Z.G. wrote the paper. All authors discussed and interpreted the data.

The author responsible for distribution of materials integral to the findings presented in this article in accordance with the policy described in the Instructions for Authors (<https://academic.oup.com/plcell>) is: Zhizhong Gong (gongzz@cau.edu.cn).

Abstract

Stomatal opening is largely promoted by light-activated plasma membrane-localized proton ATPases (PM H⁺-ATPases), while their closure is mainly modulated by abscisic acid (ABA) signaling during drought stress. It is unknown whether PM H⁺-ATPases participate in ABA-induced stomatal closure. We established that BRI1-ASSOCIATED RECEPTOR KINASE 1 (BAK1) interacts with, phosphorylates and activates the major PM Arabidopsis H⁺-ATPase isoform 2 (AHA2). Detached leaves from *aha2-6* single mutant *Arabidopsis thaliana* plants lost as much water as *bak1-4* single and *aha2-6 bak1-4* double mutants, with all three mutants losing more water than the wild-type (Columbia-0 [Col-0]). In agreement with these observations, *aha2-6*, *bak1-4*, and *aha2-6 bak1-4* mutants were less sensitive to ABA-induced stomatal closure than Col-0, whereas the *aha2-6* mutation did not affect ABA-inhibited stomatal opening under light conditions. ABA-activated BAK1 phosphorylated AHA2 at Ser-944 in its C-terminus and activated AHA2, leading to rapid H⁺ efflux, cytoplasmic alkalinization, and reactive oxygen species (ROS) accumulation, to initiate ABA signal transduction and stomatal closure. The phosphorylation-mimicking mutation AHA2^{S944D} driven by its own promoter could largely compensate for the defective phenotypes of water loss, cytoplasmic alkalinization, and ROS accumulation in both *aha2-6* and *bak1-4* mutants. Our results uncover a crucial role of AHA2 in cytoplasmic alkalinization and ABA-induced stomatal closure during the plant's response to drought stress.

IN A NUTSHELL

Background: Stomatal opening and closure are modulated by different signaling pathways in plants. Blue and red light promote stomatal opening by activating plasma membrane (PM) proton H^+ -ATPases, mainly AHA1 and AHA2, through phosphorylating their C-termini to promote proton efflux across the guard cells, thus activating the hyperpolarization-gated K^+ channel KAT1 to open stomata. ABA induces stomatal closure through activating protein kinases such as OST1/SnRK2.6, GHR1, and CDPKs, which activate SLAC1 to transport chloride and nitrate out of guard cells, followed by K^+ , which results in stomatal closure.

Question: It is well known that PM H^+ -ATPases play crucial roles in light-stimulated stomatal opening. However, it is unclear whether the PM H^+ -ATPases are also involved in ABA-induced stomatal closure.

Findings: The receptor-like protein kinase BAK1 plays an important role in ABA-induced stomatal closure. We identified in this study that BAK1 interacts with AHA2. Unexpectedly, we discovered that *aha2* mutants are insensitive to ABA-promoted stomatal closure, but not impaired in the ABA-mediated inhibition of light-promoted stomatal opening. ABA-activated BAK1 phosphorylated AHA2 at Ser-944 in its C-terminus to activate the H^+ -ATPase, which promoted a transient efflux of protons, cytoplasmic alkalinization, and the accumulation of reactive oxygen species (ROS) in the guard cells to initiate ABA signal transduction and promote stomatal closure. Our findings enhance our understanding of the role of PM H^+ -ATPases in the early ABA-induced stomatal closure signaling events that take place in guard cells.

Next steps: Our study raises some interesting questions about the biological roles of PM H^+ -ATPases in both light-promoted stomatal opening and ABA-induced stomatal closure. Further studies should explore the mechanism by which pH triggers ROS production, whether pH and the ROS pathway have parallel roles in ABA signaling, and the physiological interaction between protons and other ions in stomatal movement.

Introduction

Stomata consist of two guard cells that form a pore on the leaf surface and play key roles in controlling CO_2 uptake for photosynthesis and water evaporation. Cation and anion transporters at the plasma membrane (PM) and tonoplast control the osmotic potential of guard cells and thus stomatal movements. The proper regulation of stomatal movements is paramount for plant growth and development, as well as responses to biotic and abiotic stresses, to which multiple environmental and endogenous factors contribute (Schroeder et al., 2001; Shimazaki et al., 2007; Kim et al., 2010; Qi et al., 2018; Chang et al., 2020; Chen et al., 2020, 2021a).

Stomatal opening and closure are modulated by different signaling pathways in plants. Both blue and red light can promote stomatal opening by inducing the phosphorylation of PM proton (H^+)-ATPases (Shimazaki et al., 1986; Kinoshita and Shimazaki, 1999; Ando and Kinoshita, 2018). The two major blue light photoreceptors phototropin 1 (phot1) and phot2 are activated by auto-phosphorylation upon perceiving blue light and initiate a signaling cascade that leads to the activating phosphorylation of PM H^+ -ATPases (Shimazaki et al., 1986; Kinoshita and Shimazaki, 1999; Kinoshita et al., 2001; Takemiya et al., 2006, 2013; Inoue et al., 2008; Hiyama et al., 2017). Together with phototropins, other photoreceptors such as cryptochromes (cry1 and cry2, for blue light; Mao et al., 2005) and phytochromes (phyA and phyB, for red/far-red light; Wang et al., 2010) synergistically mediate stomatal opening. PM H^+ -ATPases are P-type ATPases as they are activated by protein

phosphorylation and need ATP to drive ion transport against steep concentration gradients. The Arabidopsis (*Arabidopsis thaliana*) genome includes 11 ATPase genes, all of which are expressed in guard cells (Ueno et al., 2005). *Arabidopsis thaliana* PLASMA MEMBRANE PROTON ATPASE1 (AHA1) and AHA2 are the two most highly expressed ATPase genes among 11 members in Arabidopsis. The *aha1 aha2* double mutant is embryo-lethal under normal laboratory conditions, indicating that PM H^+ -ATPases are essential for plant survival (Haruta et al., 2010).

14-3-3 proteins can bind to a peptide with a phosphorylated penultimate threonine residue in the extreme C-termini of AHA1 and AHA2 (Thr-948 in AHA1 and Thr-947 in AHA2), releasing the autoinhibition conferred by the C-termini and activating the ATPases (Svennelid et al., 1999; Kinoshita et al., 2001; Fuglsang et al., 2003; Zhang et al., 2004; Ueno et al., 2005; Falhof et al., 2016). PROTEIN KINASE SOS2-LIKE 5 (PKS5) also phosphorylates the Ser-931 residue of AHA2, which prevents the interaction of AHA2 with 14-3-3 proteins, thus reducing AHA2 activity (Fuglsang et al., 2007). The heat shock protein 40-like J3 interacts with and inhibits PKS5, increasing the activity of AHA2 (Yang et al., 2010), while SOS3-LIKE CALCIUM-BINDING PROTEIN3/CALCINEURIN B-LIKE7 (CBL7) interacts with and stabilizes PKS5–AHA2 interaction to further inhibit AHA2 activity (Yang et al., 2019). Activated PM H^+ -ATPases use ATP as energy to pump H^+ outside of guard cells, which hyperpolarizes the PM and generates an electrochemical gradient that drives other cations such as potassium (K^+) into guard cells. To compensate for the positively charged K^+ ,

other anions such as synthesized malate²⁻ (Dong et al., 2018), chloride, and nitrate accumulate in guard cells in response to K⁺ entry (Pandey et al., 2007). Metabolites such as glucose released from starch degradation and trehalose also contribute to the accumulation of osmolytes in guard cells (Flutsch et al., 2020; Wang et al., 2020). Together, these factors decrease the water potential of guard cells to allow water to enter the cells and raise turgor pressure, resulting in stomatal opening (Blatt, 1992; Schroeder et al., 2001; Gaxiola et al., 2007; Chen et al., 2020, 2021a; Flutsch et al., 2020). Genetic evidence in support of the critical role of PM H⁺-ATPases in stomatal opening was provided by the identification of the two dominant and constitutively active *AHA1* mutants *openstomata2* (*ost2*)-1*D* and *ost2*-2*D*, which are insensitive to almost all factors that normally promote stomatal closure, such as abscisic acid (ABA), high CO₂ concentrations, darkness, hydrogen peroxide (H₂O₂), and calcium (Ca²⁺) ions (Merlot et al., 2007). In addition, the PM-localized leucine-rich repeat receptor kinase (LRR-RLK) Plant Peptide Containing Sulfated Tyrosine 1 Receptor (PSY1R) can interact with the C-terminus of *AHA2*, phosphorylate Thr-881, and activate *AHA2*, without affecting binding by 14-3-3 proteins (Fuglsang et al., 2014). The phosphorylation of Ser-889 in *AHA1* and *AHA2* decreases their pump activity. However, it is unknown whether this phosphorylation also influences binding by 14-3-3 proteins (Nühse et al., 2007; Haruta et al., 2014).

Many components, especially those involved in ABA signaling, promote stomatal closure under drought stress conditions (Chen et al., 2021a). ABA is quickly accumulated under drought stress, which is bound by PYRABACTIN RESISTANCE 1 (PYR1)/PYR1-LIKE (PYL)/REGULATORY COMPONENT OF ABA RECEPTOR (RCAR) ABA receptors (Ma et al., 2009; Park et al., 2009). The ABA-bound PYLs competitively interact with the clade A PP2Cs, thus releasing their inhibition on SNF1-RELATED PROTEIN KINASE 2.2/3/6 (OST1; SnRK2s) (Ma et al., 2009; Park et al., 2009). Osmotic stress stimulates the B2 and B3 subfamily RAF proteins that phosphorylate and activate SnRK2s (Fabregas et al., 2020; Katsuta et al., 2020; Lin et al., 2020; Soma et al., 2020; Takahashi et al., 2020). The activated-SnRK2s either activate other SnRK2s (Lin et al., 2021b), or phosphorylate downstream targets (Chen et al., 2020, 2021a). The slow-type anion channel SLOW ANION CHANNEL-ASSOCIATED 1 (SLAC1) and the rapid-type anion channel QUICK-ACTIVATING ANION CHANNEL 1 (QUAC1, also named MALATE TRANSPORTER 12) are phosphorylated and stimulated by ABA-activated OST1 and play a major role in stomatal closure in both dicot and monocot species (Vahisalu et al., 2008; Geiger et al., 2009; Meyer et al., 2010; Imes et al., 2013; Wu et al., 2019). SLAC1 can also be activated by other kinases such as the receptor-like protein kinase GUARD CELL HYDROGEN PEROXIDE-RESISTANT1 (GHR1), CBL-INTERACTING PROTEIN KINASEs (CIPKs), and CALCIUM-DEPENDENT PROTEIN KINASEs (CPKs; Hua et al., 2012; Chen et al., 2021a). Rapid anion efflux from guard cells by

activated SLAC1 and QUAC1 channels depolarizes the PM, which activates K⁺ efflux channels and thus drives K⁺ efflux and solute release from guard cells, culminating in stomatal closure (Schroeder et al., 2001; Qi et al., 2018; Chen et al., 2020, 2021a). ABA also inhibits the blue light-mediated phosphorylation of H⁺-ATPases through the classic ABA signaling components ABA INSENSITIVE 1 (ABI1) and ABI2, two members of the protein phosphatase 2C family, as well as the kinase OST1/SnRK2.6, and therefore likely blocks blue light-stimulated stomatal opening (Hayashi et al., 2010; Yin et al., 2013). This hypothesis is further supported by the finding that ABA promotes the interaction between VESICLE-ASSOCIATED MEMBRANE PROTEIN 711 (VAMP711) and the C-terminus of *AHA1* or *AHA2*; this interaction represses *AHA1/AHA2* activity and limits stomatal closure under drought stress (Xue et al., 2018). In addition, ABI1 interacts with the C-terminus of *AHA2* and dephosphorylates the phosphorylated Thr-947 residue, inhibiting H⁺ efflux and compromising primary root growth and root hydrotropism (Miao et al., 2021).

The early stage of stomatal closure is characterized by the rapid elevation of cytosolic pH in response to ABA, which contributes to cytoplasmic alkalization and leads to the production of reactive oxygen species (ROS) and nitric oxide (NO; Suhita et al., 2004; Gonugunta et al., 2008, 2009; Islam et al., 2010). CIPKs and ABA-activated OST1 regulate ARABIDOPSIS THALIANA RESPIRATORY BURST OXIDASE HOMOLOG F NADPH oxidase to produce reactive oxygen intermediates (Sirichandra et al., 2009; Han et al., 2019). ROS accumulation can in turn enhance cytoplasmic alkalization (Zhang et al., 2001) and activate Ca²⁺ channels at the PM, raising cytosolic calcium concentrations (Schroeder and Hagiwara, 1990; Grabov and Blatt, 1998; Pei et al., 2000; Murata et al., 2001). The increase in cytosolic Ca²⁺ activates SLAC1 via several protein kinases such as CPKs and CIPKs to close stomata (Chen et al., 2021a). However, the molecular events upstream of cytosolic alkalization are not well understood.

The Arabidopsis LRR-RLK BRI-ASSOCIATED RECEPTOR KINASE 1 (BAK1, also named SOMATIC EMBRYOGENESIS RECEPTOR-LIKE KINASE 3 [SERK3]) typically functions as a co-receptor with many receptor-like protein kinases to regulate multiple signal transduction cascades involved in responses to attacks by pathogenic bacteria, drought stress, and growth and development (Li et al., 2002; Wei and Li, 2018; Wu et al., 2018; Xue et al., 2020; Zhang et al., 2020; Zhou et al., 2020). ABA-induced stomatal closure is impaired in *bak1* mutants, which is accompanied by a greater water loss in the mutants relative to the wild-type (Shang et al., 2016).

We explored the mechanism by which BAK1 regulates stomatal movement by testing whether the co-receptor might interact with ion channel proteins, and we identified *AHA2* as a candidate interacting partner. Unexpectedly, we discovered that *aha2* mutants are insensitive to ABA-promoted stomatal closure. However, *aha2* mutants are not

impaired in the inhibition of light-promoted stomatal opening by ABA. ABA activated BAK1, which in turn phosphorylated AHA2 at Ser-944 in its C-terminus and activated the H^+ -ATPase. ABA treatment promoted proton efflux in a short time in Columbia-0 (Col-0) guard cells but not in *aha2-6* or *bak1-4* mutants. In addition, ABA-induced cytoplasmic alkalinization and the accumulation of ROS were more pronounced in Col-0 than in the *aha2-6* or *bak1-4* mutants. Our findings emphasize the importance of PM H^+ -ATPases not only in light-promoted stomatal opening but also in ABA-induced stomatal closure, and provide a deeper understanding of the early signaling events taking place in guard cells in response to drought stress.

Results

BAK1 interacts with the PM H^+ -ATPase AHA2

Many ion channels located at the PM affect stomatal movement (Pandey et al., 2007). BAK1 influences ABA-mediated stomatal closure and drought tolerance (Shang et al., 2016). We sought to determine whether any ion channel participates in ABA-induced stomatal closure alongside BAK1. To this end, we first employed a luciferase complementation imaging (LCI) assay in *Nicotiana benthamiana* leaves to screen ion channel proteins for interaction with BAK1: we detected a robust luciferase signal between the *A. thaliana* PM H^+ -ATPase AHA2 and BAK1, two PM-localized proteins (Palmgren and Axelsen, 1998; Palmgren, 2001; Nam and Li, 2002), with nLUC and cLUC on the inside of the PM (Figure 1, A and C). We used β -GLUCURONIDASE (GUS) fused with cLUC or nLUC in *N. benthamiana* as a negative control: GUS failed to interact with either AHA2 or BAK1 (Figure 1, A and C). All transiently infiltrated constructs were expressed to comparable levels, as determined by endpoint RT-PCR (Figure 1B).

To validate this interaction, we next performed a co-immunoprecipitation (Co-IP) assay. We transiently co-transfected Arabidopsis protoplasts with constructs encoding AHA2-Myc and BAK1-Flag or SERK4-Flag (SERK4, a BAK1 homologous protein). Following IP of AHA2-Myc with anti-Myc antibodies, we detected BAK1-Flag among the immunoprecipitates, but not SERK4-Flag, with anti-Flag antibodies (Figure 1D), indicating that AHA2 interacts with BAK1 in planta.

To further explore their interaction, we used a dual membrane system yeast two-hybrid (Y2H) assay (Thaminy et al., 2004). We cloned the AHA2 cDNA in-frame with the *NubG* coding sequence in the prey vector pPR3-STE; we then individually co-transformed the resulting plasmid (AHA2-pPR3-STE) with the bait plasmids *PKS5*-pBT3-N (as a positive control) (Fuglsang et al., 2007), BAK1-pBT3-SUC, or *GHR1*-pBT3-STE (a PM protein; Hua et al., 2012) into yeast strain NMY51. Although all plasmid combinations grew on synthetic defined (SD) medium lacking leucine and tryptophan (–2 SD), only yeast cells harboring the pairs AHA2-pPR3-STE and BAK1-pBT3-SUC or AHA2-pPR3-STE and *PKS5*-pBT3-N grew on SD selection medium lacking leucine,

tryptophan, and histidine (–3 SD) and containing 3-mM 3-amino-1,2,4-triazole (3 AT) for high stringency (Figure 1E), suggesting that AHA2 interacts with *PKS5* and BAK1 at the membrane but not with *GHR1*. Yeast colonies with only the prey plasmids for AHA2, BAK1, or *GHR1* also failed to grow on –3 SD medium (Figure 1E), confirming the specific interaction between BAK1 and AHA2.

BAK1 has a kinase domain (KD) that displays kinase activity when purified from *Escherichia coli*, likely because bacterial kinases can phosphorylate and activate BAK1 (Li et al., 2002). The AHA2 C-terminus is an auto-inhibitory domain that represses its H^+ -ATPase activity to which several phosphorylated residues have been mapped (Palmgren et al., 1990; Fuglsang et al., 2011; Xue et al., 2018). We attempted to delineate the BAK1–AHA2 interaction peptide by Y2H using the BAK1-KD and the AHA2 C-terminus. We observed that BAK1-KD is sufficient for the interaction with the C-terminus of AHA2 (Figure 1F). The KD of the BAK1 homologous kinase SERK4 (SERK4-KD) did not sustain the growth of yeast colonies when grown on SD selection medium lacking leucine, tryptophan, histidine, and adenine (–4 SD) (Figure 1F), reinforcing the specific interaction between BAK1 and AHA2. Taken together, these results demonstrate that AHA2 interacts with BAK1 in vitro and in vivo.

AHA2 genetically functions in the same pathway as BAK1 in ABA-induced stomatal closure

To investigate whether AHA2 participates in BAK1-mediated ABA and drought responses (Shang et al., 2016), we generated the *aha2-6 bak1-4* double mutant by crossing the T-DNA insertion mutants *aha2-6* (SALK_062371) and *bak1-4* (SALK_116202) (Kemmerling et al., 2007). Rosettes of the *bak1-4*, *aha2-6*, and *aha2-6 bak1-4* mutants were a little smaller than those of the wild-type (Col-0; Figure 2A). Pots filled with the same amount of soil were first fully watered, and then put on a slowly rotating plate board under light so that the plants in each pot were uniformly illuminated. We assessed the drought tolerance phenotype of all genotypes when the 7-day-old seedlings were grown on soil for 14 days and then water was withheld for a further 16 days. Although mutant rosettes were smaller, they appeared to lose water faster than Col-0, as evidenced by an earlier appearance of drought symptoms (Figure 2B). When watered again after water withholding, only Col-0 plants recovered (Figure 2B). We also measured water loss in detached leaves taken from 4-week-old plants grown on soil. Detached leaves from all mutants (*aha2-6 bak1-4*, *aha2-6*, and *bak1-4*) exhibited similar water loss that was greater than that in the Col-0 (Figure 2C). We further compared stomatal movement in the absence or presence of ABA treatment using leaf peels that were first treated under strong light in 4-morpholineethanesulfonic acid hydrate (MES) buffer to fully open stomata. Although the stomatal apertures were comparable across all genotypes under control conditions (–ABA), *bak1-4*, *aha2-6*, and *aha2-6 bak1-4* mutants all presented wider

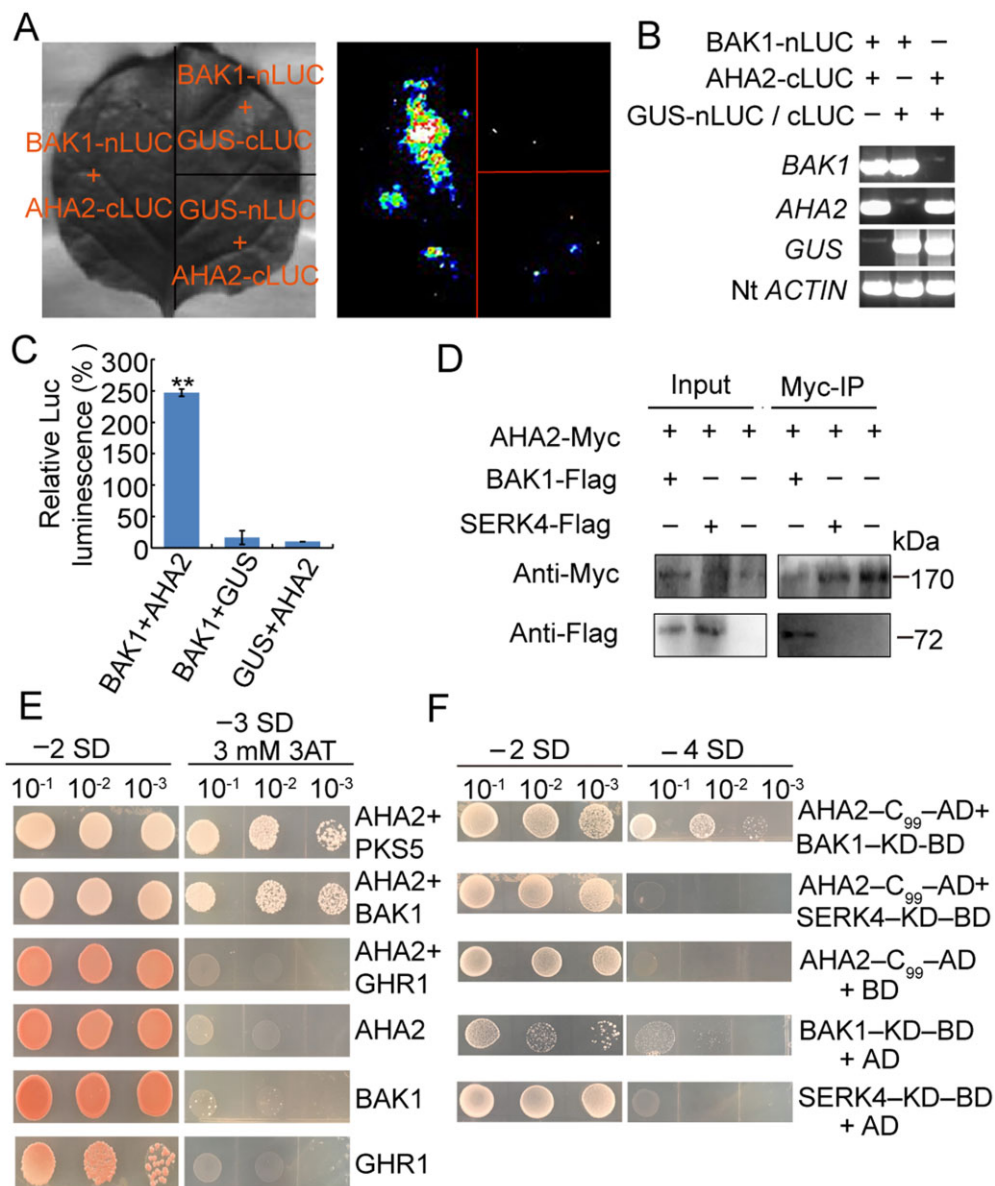


Figure 1 BAK1 interacts with the PM H⁺-ATPase AHA2. **A**, Luciferase LCI assay showing the interaction between BAK1 and AHA2 in *N. benthamiana* leaves. BAK1-nLUC and AHA2-cLUC constructs were transiently infiltrated into *N. benthamiana* leaves. GUS-nLUC and GUS-cLUC were used as negative controls. Luminescence signals (right images) were collected with a cooled CCD camera after 48–72 h. The bright field image is shown on the left. **B**, Transcript levels of BAK1, AHA2, or GUS in the transiently infiltrated *N. benthamiana* leaves shown in (A), as determined by endpoint RT-PCR. Nt ACTIN was used as a control. **C**, Comparison of Luciferase LCI from (A). Data are shown as means of three replicates; error bars represent standard deviation (SD). Significant differences compared to BAK1 + GUS, as determined by Student's *t* test: ***P* < 0.01. **D**, Co-IP assay showing the *in vivo* interaction of BAK1 and AHA2. BAK1-Flag and AHA2-Myc constructs were transfected into Arabidopsis protoplasts and cultivated for 16–18 h. IP was performed with anti-Myc antibodies and immunoprecipitates detected with anti-Flag antibodies. SERK4 is a BAK1 homolog and serves as a negative control. **E**, BAK1 interacts with AHA2 in a dual membrane system Y2H assay. Prey clone: AHA2-pPR3-STE. Bait clones: PKS5-pBT3-N (positive control), BAK1-pBT3-SUC, and GHR1-pBT3-STE (negative control). Pairs of clones were transformed into yeast strain NMY51. The resulting colonies were spotted as 10- μ L aliquots and 10 \times dilution series on SD medium lacking leucine and tryptophan (-2 SD) or on high-stringency selective medium lacking leucine, tryptophan, and histidine (-3 SD with 3 mM 3 AT) at 30°C for 3 days. **F**, The KD of BAK1 interacts with the C terminus (C₉₉) of AHA2 in a Y2H assay. SERK4 serves as negative control. -4 SD: selective medium lacking leucine, tryptophan, histidine, and adenine.

stomatal apertures than Col-0 when treated with 10 μ M ABA (Figure 2D). Taken together, these results suggest that, genetically, AHA2 and BAK1 participate in the same pathway for ABA-mediated stomatal closure under drought stress.

The constitutively active AHA1 mutant *ost2-2D* showed an impaired response to almost all factors that normally promote stomatal closure (Merlot et al., 2007). We wished to test whether *ost2-2D* and *aha2-6* affected water loss in a similar manner. We first compared drought phenotypes in

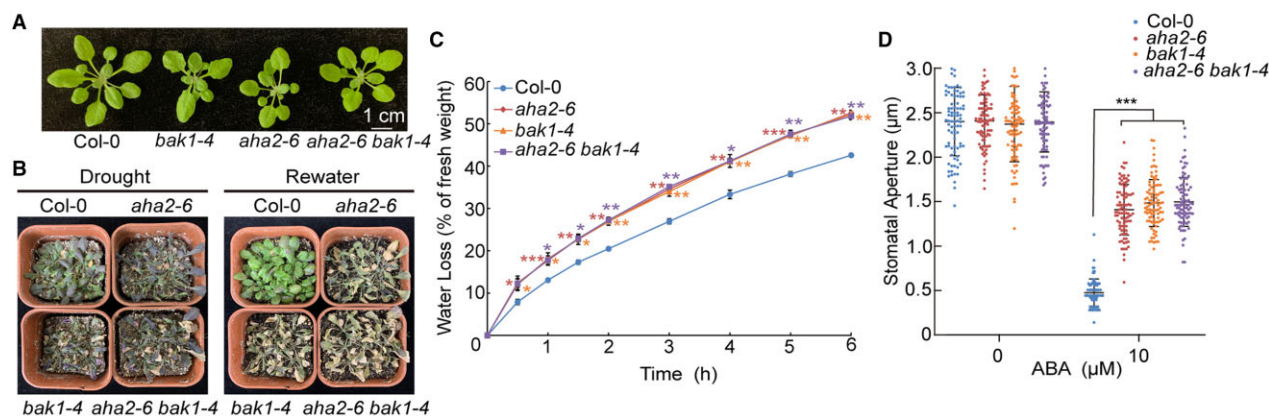


Figure 2 AHA2 and BAK1 function in the same genetic pathway in drought stress. A, Representative photographs of wild-type (Col-0), *bak1-4*, *aha2-6 bak1-4*, and *aha2-6* plants. Bar = 1 cm. B, Representative outcome of drought assays on soil-grown Col-0, *bak1-4*, *aha2-6 bak1-4*, and *aha2-6* plants. Fourteen-day-old soil-grown plants were subjected to drought stress by withholding water for about 16 days, reducing the soil moisture to 58%–55% (left), and rewatered for 3 days before the second photograph (right) was taken. C, Water loss of detached leaves of Col-0, *bak1-4*, *aha2-6 bak1-4*, and *aha2-6* plants. Detached rosette leaves of 4-week-old plants were used for water loss measurements. Data are shown as means of three replicates (five whole plants per replicate) in one experiment; error bars represent sd. Three independent experiments were performed with similar results. Significant differences compared to Col-0, as determined by Student's *t* test: **P* < 0.05, ***P* < 0.01, ****P* < 0.001. D, Stomatal aperture in ABA-induced stomatal closure assays. Epidermal peels from leaves with preopened stomata were kept in MES-KOH buffer for 4 h or MES-KOH buffer containing 10- μM ABA for another 2 h before data acquisition. Data are shown as means of three replicates (30 stomata from two rosette leaves per replicate) from one representative experiment; error bars represent sd. Three independent experiments were performed with similar results. Significant differences compared to Col-0 under the same treatment, as determined by Student's *t* test: ****P* < 0.001.

the Col-0 and the *aha2-6* and *ost2-2D* mutants. When water was withheld from plants growing on soil, *ost2-2D* and *aha2-6* mutants exhibited drought symptoms earlier than the Col-0, with *ost2-2D* even earlier than *aha2-6* (Figure 3A, top). Following rewatering after prolonged exposure to drought, only the Col-0 plants recovered (Figure 3A, bottom). The leaf surface temperature reflects the stomatal transpiration rate, with higher transpiration accompanying lower temperature (Hua et al., 2012). We next conducted an infrared thermal imaging assay to detect leaf surface temperature. *ost2-2D* mutants had lower leaf surface temperatures than *aha2-6*, both of which had a significantly lower temperature than the wild-type (Figure 3, B and C). We further performed a stomatal conductance assay under ABA treatment. The stomatal conductance of *aha2-6* was larger than the wild-type plants after 5- μM ABA was sprayed on the leaf surface (Figure 3D). Similarly, photosynthetic rates of *aha2-6*, *bak1-4*, *aha2-6 bak1-4* and *ost2-2D* were higher than that of the wild-type plants when subjected to drought stress. However, *ost2-2D* had a steadily high photosynthetic rate before drought stress, and the other mutants had similar photosynthetic rates as the wild-type (Figure 3E). We then quantified the extent of water loss over a 24-h diurnal cycle in soil-grown plants by weighing pots every 5 min for three continuous days as described previously (Hua et al., 2012): during the light part of the cycle, both the *aha2-6* and *ost2-2D* mutants lost more water than Col-0 plants, but the water loss of *ost2-2D* was much more pronounced than that of *aha2-6* (Figure 3F). In the dark, water loss was similar between the *aha2-6* and Col-0 plants, but *ost2-2D* still lost more water than *aha2-6* or Col-0 (Figure 3F). In the detached leaf assay, *ost2-2D* leaves showed a remarkably fast

loss of water compared to *aha2-6* and Col-0 leaves, although *aha2-6* leaves lost water faster than Col-0 leaves (Figure 3G). We then conducted an ABA-promoted stomatal closure assay using leaf peels, which revealed that fully opening stomata in *ost2-2D* showed little response to ABA treatment, as previously reported (Merlot et al., 2007). In the same assay, *aha2-6* stomata exhibited an intermediate response between that of Col-0 and *ost2-2D* (Figure 3H). *ost2-2D* also completely abolished the inhibition of light-induced stomatal opening by ABA (Merlot et al., 2007), whereas both Col-0 and *aha2-6* responded normally (Figure 3I). These results indicate that *aha2-6* only impairs ABA-induced stomatal closure but does not affect the inhibition of light-induced stomatal opening by ABA, which is different from *ost2-2D*.

To further confirm the *aha2-6* phenotype, we phenotyped an additional *aha2-4* allele (Supplemental Figure S1A). We compared the stomata density on the leaves of the *aha2-6* mutant and Col-0 plants and observed no differences (Supplemental Figure S1B). We confirmed that all the *aha2-6* phenotypes described above were also observed in *aha2-4* including plant growth on soil under drought stress, detached leaf water loss assay, ABA-induced stomatal closure, and ABA-mediated inhibition of light-induced stomatal opening (Supplemental Figure S1, C–F). The observed phenotypes were not due to transcriptional changes in the remaining AHA genes (Supplemental Figure S1, G and H). We also introduced a complementation construct *ProAHA2:AHA2* into the *aha2-6* mutant background. Although relative AHA2 transcript levels in the resulting transgenic lines were similar to those in Col-0 (Supplemental Figure S2A), transgenic lines *ProAHA2:AHA2/aha2-6* #2 and *ProAHA2:AHA2/aha2-6* #4 only showed

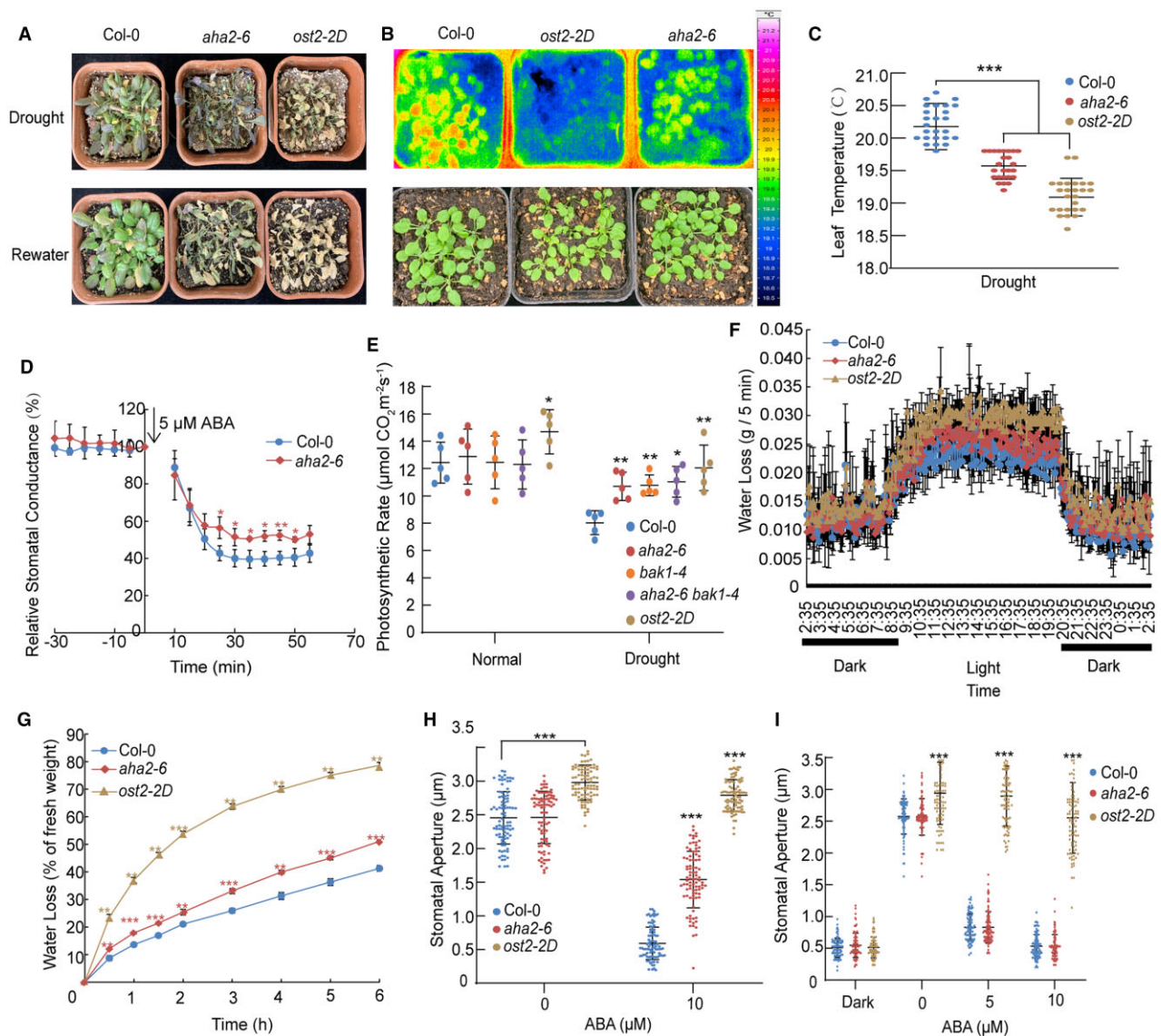


Figure 3 AHA2 positively regulates ABA-induced stomatal closure. **A**, Representative outcome of drought assays on soil-grown Col-0, *aha2-6*, and *ost2-2D* plants. Fourteen-day-old soil-grown plants were subjected to drought stress by withholding water for about 16 days, during which the soil moisture was reduced to 58%–55% (top), and rewatered for 3 days before the photograph (bottom). **B**, Infrared thermal imaging assay on the leaf temperature of soil-grown Col-0, *aha2-6*, and *ost2-2D* plants (top). Ten-day-old soil-grown plants were photographed by Infrared thermal imager when soil moisture was 80%–75%. The pseudocolor bar represents the range of temperature. The bottom image was photographed in bright filed. **C**, Comparison of the leaf temperature from (**B**). Data are shown as means of three replicates (nine plants in one pot per replicate), error bars represent SD ; Statistical significance compared to Col-0, as determined by Student's *t* test: *** $P < 0.001$. **D**, Stomatal conductance of Col-0 and *aha2-6* plants in response to the ABA. About 3- to 4-week-old Col-0 and *aha2-6* plants were used for sustaining recording stomatal conductance for 100 min. The stimulus (5- μM ABA) was applied at the point zero. Data are shown as means of three replicates (one seedling per replicate) in one experiment. Error bars represent SD . The experiment was repeated 3 times with similar results. Significant differences compared to Col-0, as determined by Student's *t* test: * $P < 0.05$, ** $P < 0.01$. **E**, Photosynthetic rate of Col-0, *aha2-6*, *bak1-4*, *aha2-6 bak1-4*, and *ost2-2D* plants. Fourteen-day-old soil-grown plants were analyzed using a LI-6400XT portable photosynthesis system when soil moisture was 95%–90% (Normal). Then, water was withheld until the soil moisture reached 80%–75%, and the second measurement was taken (Drought). Data are shown as means of five replicates (one seedling per replicate) in one experiment. Error bars represent SD . The experiment was repeated 3 times with similar results. Significant differences compared to Col-0 under the same treatment, as determined by Student's *t* test: * $P < 0.05$, ** $P < 0.01$. **F**, Water loss for Col-0, *aha2-6*, and *ost2-2D* plants grown on soil over 24 h. Water loss was determined by weighing pots every 5 min for 3 days. Values are means of three replicates in one experiment, each replicate being one pot with five seedlings per pot; error bars represent SD . During the day, *aha2-6* lost more water ($P < 0.05$) than Col-0; *ost2-2D* lost more water ($P < 0.001$) than Col-0. During the night, *ost2-2D* lost more water ($P < 0.05$) than Col-0 and *aha2-6*, while Col-0 and *aha2-6* lost similar amounts of water, Student's *t* test. Three independent experiments were performed with similar results. **G**, Water loss from detached leaves of Col-0, *aha2-6*, and *ost2-2D* plants. Data are shown as means of three replicates (five seedlings per replicate) from one experiment; error bars represent SD . Three independent experiments were performed with similar results. Significant differences compared to Col-0, as determined by Student's *t* test: ** $P < 0.01$, *** $P < 0.001$. **H**, ABA-induced stomatal closure in Col-0, *aha2-6*, and *ost2-2D* plants.

(continued)

partial rescue, as evidenced by water loss in detached leaves and ABA-induced stomatal closure (Supplemental Figure S2, B and C). One possible explanation might stem from interference of transgenic AHA2 by a predicted truncated AHA2 protein produced in *aha2-6* plants. However, we did not detect any differences between Col-0 and *aha2* mutants with respect to ABA-inhibited primary root growth or seed germination (Supplemental Figure S3, A–D), suggesting that AHA2 is not involved in ABA responses in seedlings. Taken together, our results suggest that AHA2 is a positive regulator of ABA-induced stomatal closure.

ABA enhances phosphorylation of the AHA2-C-terminus by BAK1

Since BAK1 interacts with AHA2, BAK1 may directly phosphorylate AHA2. To test this hypothesis, we performed a protein kinase assay. We treated transgenic plants from a Super promoter driving *BAK1-FLAG/bak1-4* complemented line with 50- μ M ABA or only 1/2 Murashige and Skoog (MS) culture medium as a mock control for 30 min before pulling down BAK1 with anti-Flag antibodies. We then incubated the immunoprecipitates with recombinant glutathione S-transferase (GST)-AHA2-C₉₉ (corresponding to the last 99 amino acids of AHA2) for 30 min at 30°C in the presence of 1 μ Ci [γ -³²P] ATP. BAK1 activity was enhanced by ABA treatment, and BAK1 phosphorylated AHA2-C₉₉, and this phosphorylation was enhanced by ABA treatment (Figure 4, A and B). However, we also observed basal phosphorylation levels in the *bak1-4* mutant, possibly from other nonspecific kinase(s) pulled-down with the Flag beads during IP. This result suggests that BAK1 can phosphorylate the C-terminus of AHA2, which is enhanced by ABA treatment.

The phosphorylation sites of AHA2 in Thr-881, Ser-899, Ser-904, Ser-931, Ser-944, Tyr-946, Thr-947, and Ser-904 have been identified in previous studies (Nühse et al., 2007; Rudashevskaya et al., 2012). Next, we introduced several point mutations in the AHA2 C-terminus, changing Ser/Thr or Tyr residues to Ala to mimic a nonphosphorylated form of AHA2, and repeated the in vitro phosphorylation assay with recombinant BAK1-KD. The autoradiograph signals derived from AHA2^{S944A}, AHA2^{T881A}, AHA2^{T858A}, and AHA2^{Y946A} were lower than that derived from the intact AHA2 C-terminus, with only a weaker signal detected when all four sites were mutated to Ala, indicating that they are all likely phosphorylated by BAK1-KD in vitro (Figure 4, C and D). Since the phosphorylation signal of AHA2^{S944A} was

the lowest among the four individual mutated sites, we mainly focused on AHA2^{S944} hereafter.

We purified the BAK1-KD from *E. coli* and incubated the recombinant protein with AHA2-C₉₉ in the presence of ATP. Using a specific antibody recognizing the phosphorylated AHA2^{S944} peptide (pAHA2^{S944}) for immunoblot analysis, we detected two phosphorylated bands from the reactions between BAK1-KD and AHA2-C₉₉, but not when BAK1-KD was incubated with GST (as a negative control). We also observed this lower band with AHA2-C₉₉ alone, likely because of its phosphorylation by other kinase(s) from *E. coli* (Figure 4, E and F) and/or a nonspecific cross reacting one. We next validated the phosphorylation of AHA2^{S944} by BAK1 in vivo. We treated 10-day-old Col-0 and *bak1-4* seedlings with 50- μ M ABA for 0, 15, 30, or 60 min before protein extraction and immunoblot analysis with anti-ATPase antibodies (as a loading control) and anti-pAHA2^{S944} antibodies. The intensity of the band detected with the anti-AHA2^{S944} antibody was stronger in Col-0 seedlings treated with ABA relative to without ABA control or relative to *bak1-4* at 30 and 60 min (Figure 4, G and H), indicating that ABA induces the phosphorylation of AHA2^{S944} by BAK1 in vivo, and the phosphorylation level was highest at 30 min among the time points examined. In another experiment, we confirmed the phosphorylation of AHA2^{S944}, but did not find the apparent phosphorylation intensity change of *aha2-6* or *bak1-4* after ABA treatment for 30 min (Figure 4, I and J). The weak phosphorylation signal detected using AHA2^{S944} antibodies was also detected in the *aha2-6* or *bak1-4* mutant, which may be attributed to a nonspecific cross-reaction of the antibodies (Figure 4I). Thus, we repeatedly confirmed that ABA-activated BAK1 phosphorylates the AHA2 C-terminus in vivo at Ser-944.

BAK1 positively regulates AHA2 activity

Next, we investigated the biological significance of AHA2 phosphorylation by BAK1. PM H⁺-ATPases are active transporters that utilize ATP as energy to transport H⁺ across the PM (Sondergaard et al., 2004; Gaxiola et al., 2007; Duby et al., 2009). We, therefore, assessed whether BAK1 might regulate PM H⁺-ATPase activity using a PM H⁺-ATPase assay (Yang et al., 2010). We measured the PM H⁺-ATPase activity of Arabidopsis PM vesicles of Col-0 and *aha2-6* plants after incubation with recombinant BAK1-KD or GST (as a negative control) for 30 min at room temperature. After the addition of ATP, PM H⁺-ATPases hydrolyze ATP, the

Figure 3 (Continued)

The experiments were conducted as in Figure 2D. Data are means of three replicates (30 stomata from two rosette leaves per replicate) from one experiment; error bars represent SD. Three independent experiments were performed with similar results. Significant differences compared to Col-0 under the same treatment, as determined by Student's *t* test: ****P* < 0.001. I, Effects of ABA on light-induced stomatal opening in Col-0, *aha2-6*, and *ost2-2D* plants. The 4-week-old plants kept in the dark for 24 h to close their stomata were soaked in MES-KOH buffer with different concentrations of ABA (5 or 10 μ M) followed by 2-h illumination to promote stomatal opening. Stomatal apertures were measured using images acquired with a 40 \times objective light microscope. Data are shown as means of three replicates (30 stomata from two rosette leaves per replicate) from one representative experiment, error bars represent SD. Three independent experiments were performed with similar results. Significant differences compared to Col-0 under the same treatment, as determined by Student's *t* test: ****P* < 0.001.

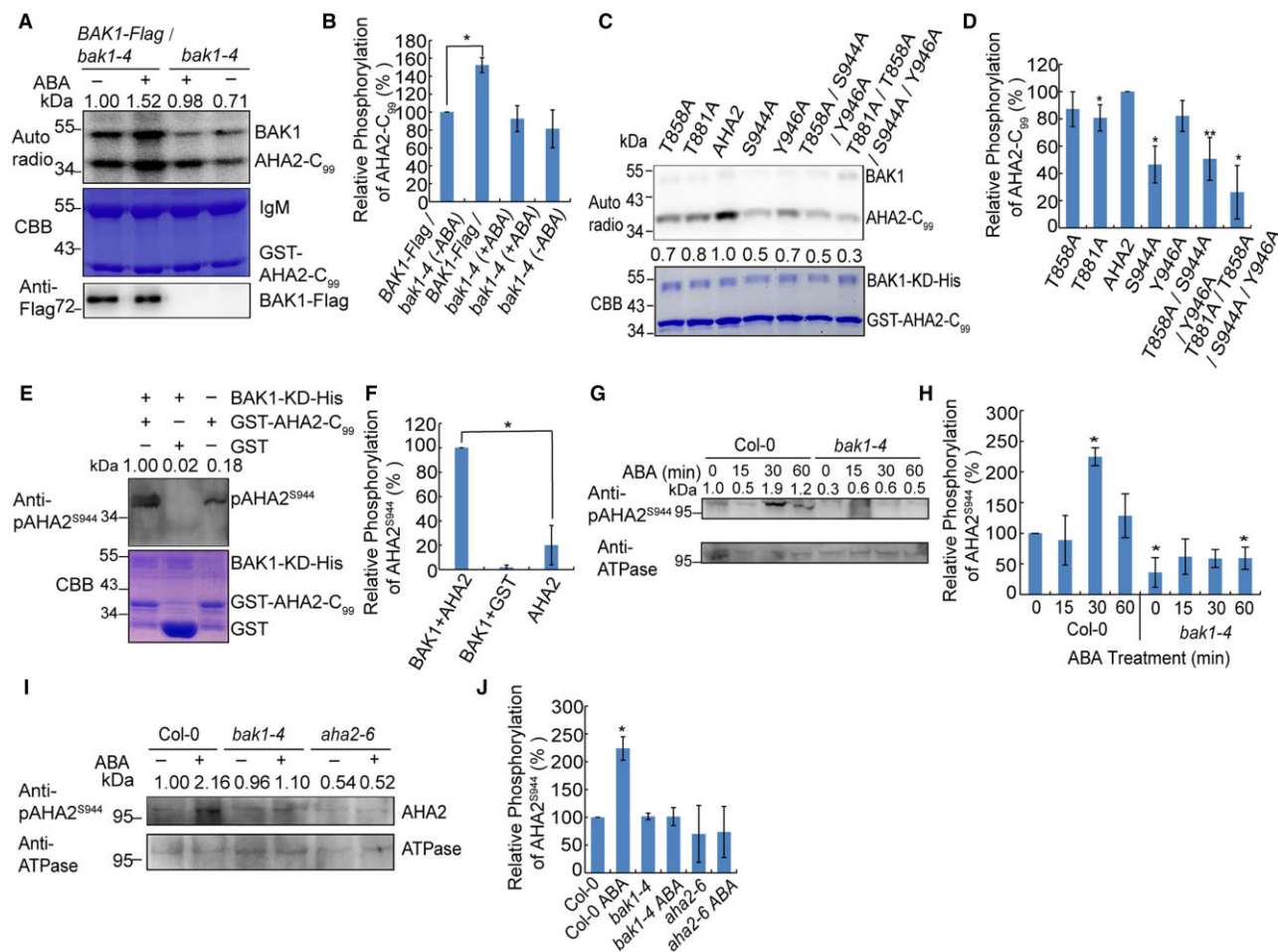


Figure 4 BAK1 phosphorylates the C-terminus of AHA2. **A**, ABA enhances the phosphorylation of the AHA2-C-terminus by BAK1. BAK1-Flag was immunoprecipitated from *bak1-4* or a super promoter driving *BAK1:BAK1-Flag/bak1-4* transgenic plants treated or not with 50- μ M ABA for 30 min using anti-Flag antibodies. Immunoprecipitates and recombinant GST-AHA2-C₉₉ purified from *E. coli* were incubated in kinase reaction buffer with 1 μ Ci [γ -³²P] ATP for 30 min at 30°C and separated by sodium dodecyl sulfate-polyacrylamide gel electrophoresis (SDS-PAGE). Top, Autoradiograph; middle, Coomassie Brilliant Blue (CBB) staining; bottom, BAK1-Flag as equal loading control, as detected by anti-Flag antibodies. Numbers represent the relative phosphorylation intensity. **B**, Statistical analyses of phosphorylation band intensity in (A). Data are means of band intensities from four independent experiments as determined by ImageJ software. Significant differences compared to without ABA treatment in *BAK1-Flag/bak1-4* plants as determined by Student's *t* test: **P* < 0.05. **C**, BAK1 phosphorylates several sites of the AHA2-C-terminus. Recombinant BAK1-KD-His protein was incubated with various recombinant AHA2 proteins in kinase reaction buffer at 30°C for 30 min and separated by SDS-PAGE. Top, Autoradiograph; bottom, CBB staining. Numbers represent relative phosphorylation intensity. **D**, Statistical analyses of phosphorylation band intensity in (C). Data are means of band intensities from three independent experiments as determined using ImageJ software. Significant differences compared to AHA2 as determined by Student's *t* test: **P* < 0.05; ***P* < 0.01. **E**, BAK1 phosphorylates AHA2^{S944} in vitro. Recombinant proteins were incubated in kinase reaction buffer in the presence of ATP and separated by SDS-PAGE. AHA2 phosphorylation status was determined with an anti-pAHA2^{S944} antibody (top). Bottom, CBB staining. Numbers represent relative phosphorylation intensity. **F**, Statistical analyses of phosphorylation band intensity in (E). Data are means of band intensities from three independent experiments as determined by ImageJ software. Significant differences compared to BAK1 + AHA2 as determined by Student's *t* test: **P* < 0.05. **G**, BAK1 phosphorylates AHA2^{S944} in vivo during ABA treatment at different timepoints. Col-0 and *bak1-4* seedlings were treated with 50- μ M ABA for 0, 15, 30, or 60 min, respectively. Total proteins were separated by SDS-PAGE, followed by immunoblotting with anti-pAHA2^{S944} antibody to determine the AHA2 phosphorylation status (top). Bottom, PM H⁺-ATPase as equal loading control, as detected by anti-ATPase antibody. Numbers represent relative phosphorylation intensity. **H**, Statistical analyses of phosphorylation band intensity in (G). Data are means of band intensities from three independent experiments as determined by ImageJ software. Significant differences compared to the wild-type Col-0 without ABA treatment as determined by Student's *t* test: **P* < 0.05. **I**, Comparison of AHA2^{S944} phosphorylation level among the wild-type, *bak1-4* and *aha2-6*. The seedlings were treated with 50- μ M ABA for 30 min. The proteins were used for immunoblotting with anti-pAHA2^{S944} antibody. Bottom, PM H⁺-ATPase as equal loading control, as detected by anti-ATPase antibody. Numbers represent relative phosphorylation intensity. **J**, Statistical analyses of phosphorylation band intensity in (I). Data are means of band intensities from three independent experiments as determined by ImageJ software. Significant differences compared to the wild-type Col-0 without ABA treatment as determined by Student's *t* test: **P* < 0.05.

resulting H^+ efflux can be quantified with the pH-sensitive fluorescent probe quinacrine, and the activity of PM H^+ -ATPases can be measured based on the quinacrine fluorescence signal (Yang et al., 2010). When recombinant BAK1-KD was added to Col-0 PM vesicles, H^+ -ATPase activity increased by about 20% within 40 s compared to the GST control, which was higher than that of recombinant BAK1-KD or GST in *aha2-6* PM vesicles (Figure 5, A and B), suggesting that BAK1-KD activates H^+ -ATPase activity in vitro.

AHA2 functions with or downstream of BAK1 in ABA-induced stomatal closure in Arabidopsis

To further explore the biological function of BAK1-mediated phosphorylation and activation of AHA2 in ABA-induced stomatal closure, we generated transgenic lines in the *aha2-6* mutant background by introducing the sequence encoding the C-terminally mutated AHA2 versions AHA2^{S944D} (phosphorylation mimetic) and AHA2^{S944A} (nonphosphorylatable) under the control of the AHA2 promoter. Transgenic expression of AHA2^{S944D} in the *aha2-6* background (i.e. in *ProAHA2:AHA2^{S944D}/aha2-6* plants) fully rescued the *aha2-6* mutant phenotypes of water loss in the detached leaf assay and ABA-induced stomatal closure, whereas transgenic expression of AHA2^{S944A} (in *ProAHA2:AHA2^{S944A}/aha2-6* plants) did not (Figure 6, A and C). Considering that the *ProAHA2:AHA2* transgene only partially complemented the *aha2-6* mutant, these results indicate that AHA2^{S944} is critical for AHA2 function in ABA-induced stomatal closure and drought stress.

To determine where AHA2 acts relative to BAK1, we also introduced the *ProAHA2:AHA2^{S944D}* and *ProAHA2:AHA2^{S944A}* transgene into the *bak1-4* mutant, respectively, and measured the water loss and ABA-mediated stomatal movement in the resulting transgenic lines. *ProAHA2:AHA2^{S944A}* expression did not have any effect on *bak1-4* in either the

detached leaf water loss or ABA-induced stomatal closure assays (Figure 6, B and C). However, *ProAHA2:AHA2^{S944D}* expression largely rescued the greater water loss normally seen in *bak1-4* in the detached leaf assay, as well as ABA-induced stomatal closure (Figure 6, B and C). These results suggest that AHA2 acts at the same level in the signaling cascade as BAK1, or downstream of BAK1, in regulating ABA-mediated drought stress responses and that the phosphorylation of Ser-944 is required for AHA2 activation. Nevertheless, these results also suggest that the phosphorylation mimetic form AHA2^{S944D} is not sufficient for promoting stomatal closure under normal growth conditions, but needs some additional component(s) in ABA-promoting stomatal closure when BAK1 is absent.

AHA2 and BAK1 are involved in ABA-mediated cytoplasmic alkalinization

Stomatal closure requires anions and cations to be transported out of guard cells across the PM. To investigate the role of AHA2 and its activation by BAK1 in ABA-induced transmembrane ion efflux in the PM of guard cells, we compared H^+ transport in the guard cells of Col-0, *aha2-6*, *bak1-4*, and *ost2-2D* plants. To measure H^+ flux, we used a self-referencing microelectrode technique, named noninvasive micro-test technique (NMT), which allows the continuous measurement of H^+ flux for 720 s from single guard cell based on Fick's first law of diffusion (Yan et al., 2015). The instantaneous application of 30 μ M ABA to the bath after 180 s caused an apparent transmembrane H^+ efflux in Col-0 and *ost2-2D* guard cells, with *ost2-2D* experiencing a stronger efflux and a faster decline than Col-0, although *ost2-2D* is characterized by its constitutive PM H^+ -ATPase activity (Figure 7A). After ABA treatment, H^+ efflux from the peak rapidly returned to near baseline levels (Figure 7A). The quantification of H^+ efflux before exposure to ABA, at the peak response and end-exposure showed that a large amount of H^+ was pumped from the cytosol to the apoplast during the peak response period in Col-0 and *ost2-2D* guard cells (Figure 7B). In sharp contrast, transmembrane H^+ flux showed no response to ABA in *aha2-6* and *bak1-4* guard cells (Figure 7, A and B). These results suggest that ABA can quickly induce a transient H^+ efflux in guard cells, which requires both BAK1 and AHA2.

ABA induces cytoplasmic alkalinization, which precedes ROS production and leads to stomatal closure (Suhita et al., 2004). Based on the H^+ efflux measured above, we wished to assess whether this transient H^+ efflux across the PM would cause a change in cytoplasmic pH. We first generated a standard curve for a range of pH values from pH 5.5 to pH 7.5 using confocal pH mapping with the ratiometric probe carboxy-seminaphthorhodafluor-1-acetoxymethylester (carboxy-SNARF-1-AM; Figure 7C). With the aid of this standard curve, we then measured pH in Col-0 and our various mutants and transgenic lines. Cytoplasmic pH was lower in both the *aha2-6* and *bak1-4* mutants relative to Col-0 under normal conditions; among them, *bak1-4* showed the lowest

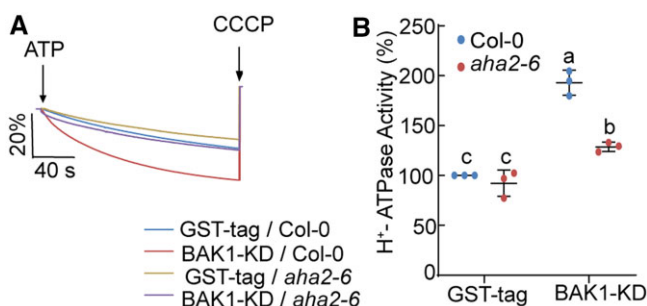


Figure 5 BAK1 positively regulates AHA2 activity. A, BAK1 enhances PM H^+ -ATPase activity in vitro. Fifty nanograms of PM vesicles from Col-0 and *aha2-6* plants were incubated with 10 μ g of recombinant BAK1-KD protein or GST (as control) for 30 min at room temperature to measure ATPase activity. B, Comparison of PM H^+ -ATPase activity from (A). Error bars represent SD. Statistical significance is indicated by different lowercase letters and was determined by Student's *t* test ($P < 0.05$). One representative experiment with three technical replicates is shown, and three independent experiments were performed with similar results.

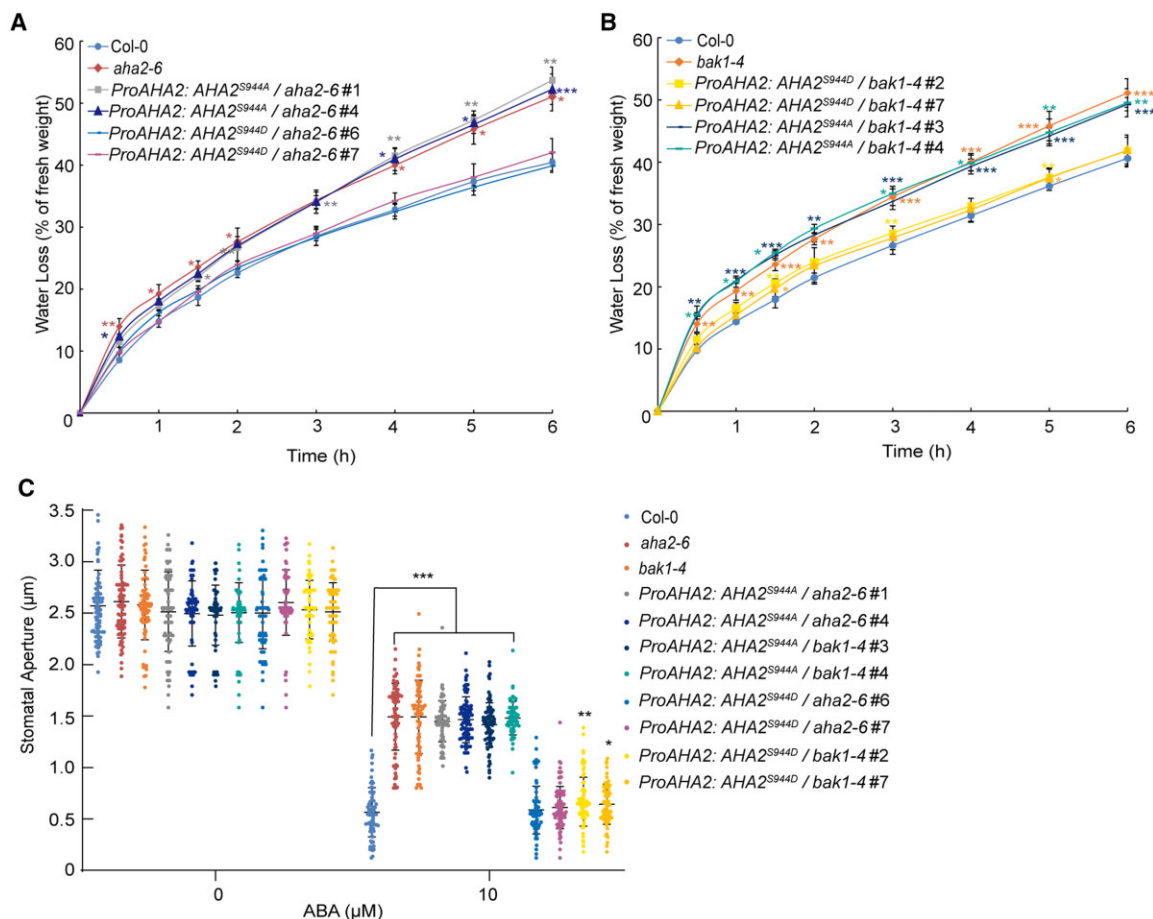


Figure 6 The phosphorylation mimetic AHA2^{S944D} fully or largely complements the water loss phenotypes of *aha2-6* or *bak1-4*, respectively. **A**, Comparison of water loss from detached leaves of Col-0, *aha2-6*, two transgenic *ProAHA2: AHA2^{S944D} / aha2-6* lines, and two *ProAHA2: AHA2^{S944A} / aha2-6* lines. The experiment is as described in Figure 2C. Error bars represent s.d. Significant difference compared to Col-0, as determined by Student's *t* test: **P* < 0.05, ***P* < 0.01, ****P* < 0.001. **B**, Comparison of water loss from detached leaves of Col-0, *bak1-4*, two transgenic *ProAHA2: AHA2^{S944D} / bak1-4* lines, and two *ProAHA2: AHA2^{S944A} / bak1-4* lines. Error bars represent s.d. Significant difference compared to Col-0, as determined by Student's *t* test: **P* < 0.05, ***P* < 0.01, ****P* < 0.001. **C**, Comparison of ABA-induced stomatal closure in Col-0, *aha2-6*, *bak1-4*, and transgenic lines as in (A) and (B). The experiment is described in Figure 2D. Error bars represent s.d. Significant difference compared to Col-0 under the same treatment, as determined by Student's *t* test: **P* < 0.05, ***P* < 0.01, ****P* < 0.001.

pH. Treatment with ABA caused a rise in cytoplasmic pH within a few minutes, but to a lesser extent in the *aha2-6* and *bak1-4* mutants compared to the Col-0 (Figure 7, D and E). In contrast, cytoplasmic pH was higher in *ost2-2D*, *ProAHA2: AHA2^{S944D} / aha2-6*, and *ProAHA2: AHA2^{S944D} / bak1-4* transgenic plants than in Col-0 before ABA treatment. ABA treatment further increased the cytoplasmic pH in the wild-type, *ProAHA2: AHA2^{S944D} / aha2-6*, and *ProAHA2: AHA2^{S944D} / bak1-4* transgenic plants, reaching a comparable level as in *ost2-2D*, which did not exhibit a difference in pH before and after ABA treatment (Figure 7, D and E). The cytoplasmic pH in *ProAHA2: AHA2^{S944A} / aha2-6* did not change after ABA treatment, while the cytoplasmic pH in *ProAHA2: AHA2^{S944A} / bak1-4* plants after ABA treatment reached a similar level as Col-0 before ABA treatment (Figure 7, D and E). It should be noted that the measured value for each pair of guard cells varies widely; the statistical analysis basically reflects the cytoplasmic pH change in different genotypes. These results

suggest that AHA2 and BAK1 participate in ABA-induced cytoplasmic alkalization.

AHA2 and BAK1 act upstream of ABA-induced ROS production and Ca²⁺ in guard cells

Since AHA2 affects cytoplasmic pH, we wondered whether it would also influence ROS accumulation. We first conducted stomatal conductance assays under ozone (O₃) treatment, which increases cellular ROS levels (Horak et al., 2016). A high concentration of O₃ (400 ppb) reduced stomatal conductance in both *aha2-6* and Col-0 to a similar extent (Supplemental Figure S4A). Similarly, stomatal closure of *aha2-6* and *aha2-4* responded normally (as observed in Col-0 plants) to H₂O₂ (Figure S4B). However, only *ost2-2D* largely abolished H₂O₂-mediated stomatal closure, as previously reported (Merlot et al., 2007). These results suggest that PM H⁺-ATPases act upstream of ROS to induce stomatal closure.

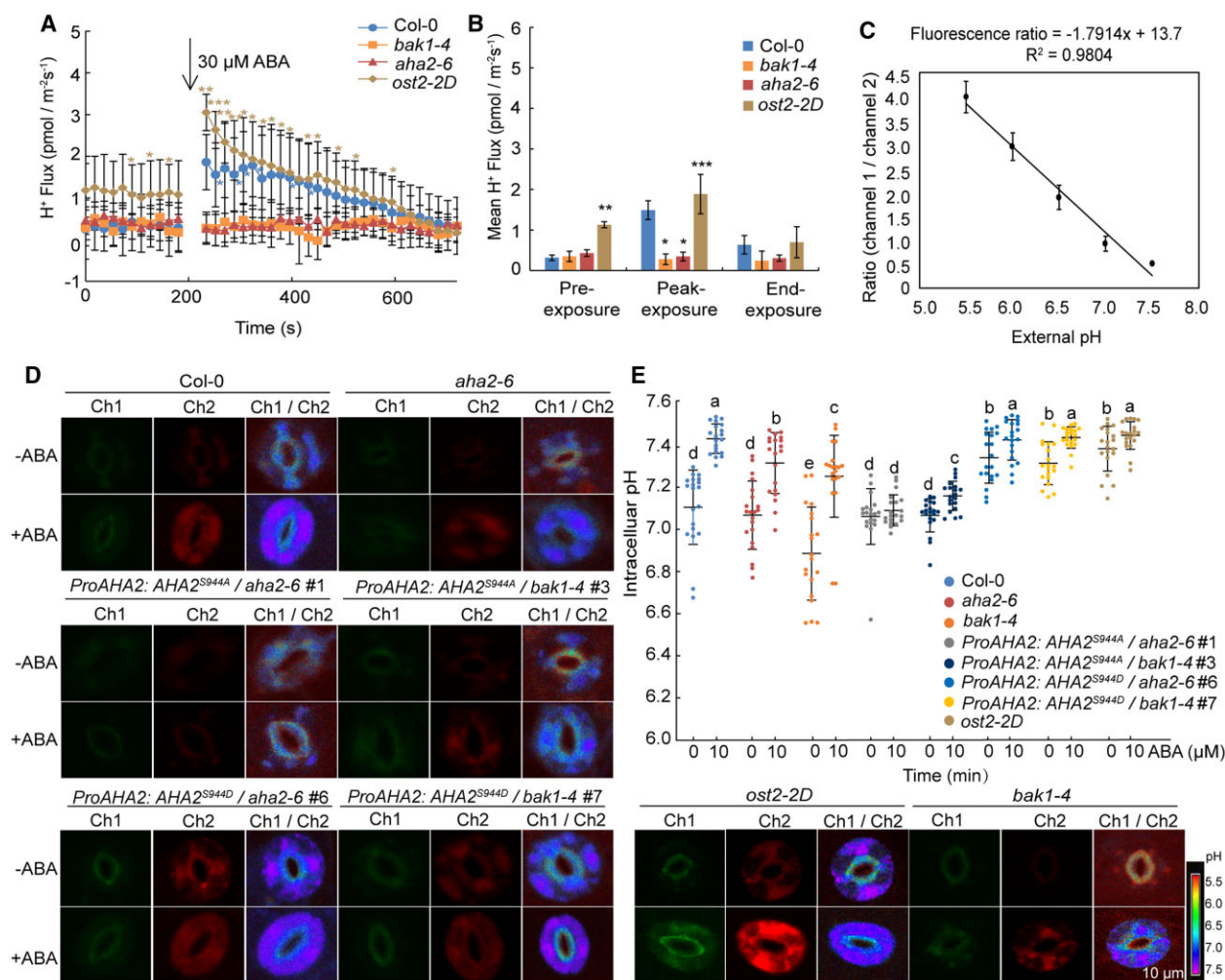


Figure 7 AHA2 and BAK1 participate in ABA-mediated cytoplasmic alkalinization. **A**, Effects of ABA addition on H^+ flux in the guard cells of Col-0, *aha2-6*, *bak1-4*, and *ost2-2D* plants. A continuous H^+ flux recording over 720 s was conducted for each guard cell in test medium, and 30- μ M ABA was added after 180 s. Each point represents the mean of six individual guard cells from one experiment and error bars represent sd. Significant difference compared to *bak1-4* as determined by Student's *t* test: * $P < 0.05$, ** $P < 0.01$, *** $P < 0.001$. Two independent experiments with six guard cells and one experiment with three guard cells were performed with similar results. **B**, H^+ flux in (A) from one experiment with six guard cells. Preexposure, 0–180 s; Peak-exposure, 181–486 s; End-exposure, 487–720 s. Error bars represent sd. Significant difference compared to Col-0 at the same stage, as determined by Student's *t* test: * $P < 0.05$, ** $P < 0.01$, *** $P < 0.001$. **C**, Calibration curve of pH-dependent fluorescence for carboxy-SNARF-1-AM dye. This dye was added to buffer containing epidermal strips. Fluorescence intensity ratios were averaged from at least five values, each representing the mean intensity ratio of an area over the entire guard cell tested. Error bars represent sd. **D**, Representative images of fluorescence intensity of cytosolic pH in guard cells of Col-0, *aha2-6*, *bak1-4*, and *ost2-2D*, one transgenic line expressing *ProAHA2: AHA2^{S944A}* in the *aha2-6* or *bak1-4* backgrounds and one transgenic line expressing *ProAHA2: AHA2^{S944D}* in the *aha2-6* or *bak1-4* backgrounds treated with or without 10- μ M ABA for 10 min. Ch1 (channel 1, Emission 580 nm); Ch2 (channel 2, Emission > 600 nm); Ch1/Ch2 (ratio of channel 1/channel 2). The pseudocolor bar represents a pH range from about 5.5–7.5 in the cytoplasmic area. Bar = 10 μ m (for all panels). **E**, Intracellular pH from 20 guard cells shown in (D). Error bars represent sd. Significant differences represented by different lowercase letters as determined by Student's *t* test ($P < 0.05$). Three independent experiments were performed with similar results.

To test this hypothesis, we measured ABA-induced ROS accumulation in seedlings using 3',3'-diaminobenzidine (DAB) staining for H_2O_2 levels and Nitro blue tetrazolium (NBT) staining for superoxide ($O_2^{\cdot-}$) levels in all genotypes. Col-0 and *ProAHA2: AHA2/aha2-6* seedlings produced more H_2O_2 and $O_2^{\cdot-}$ after ABA treatment, unlike *aha2-6* and *bak1-4* (Figure 8, A–D). In contrast to *aha2-6*, *ost2-2D* accumulated more H_2O_2 and $O_2^{\cdot-}$ even without ABA treatment compared to Col-0, which was further enhanced after ABA

treatment (Figure 8, A–D) and is consistent with the higher H^+ efflux after ABA treatment observed in this mutant (Figure 7A). We further detected the change of ROS in guard cells by a fluorochrome DCFH-DA (Hua et al., 2012). Treatment with 30- μ M ABA for 2 h induced ROS accumulation, but to a lower level in the *aha2-6* and *bak1-4* mutants compared to the Col-0 (Figure 8, E and F). In contrast, ROS in guard cells accumulated to higher levels in *ost2-2D*, *ProAHA2: AHA2^{S944D}/aha2-6*, and *ProAHA2: AHA2^{S944D}/bak1-4*

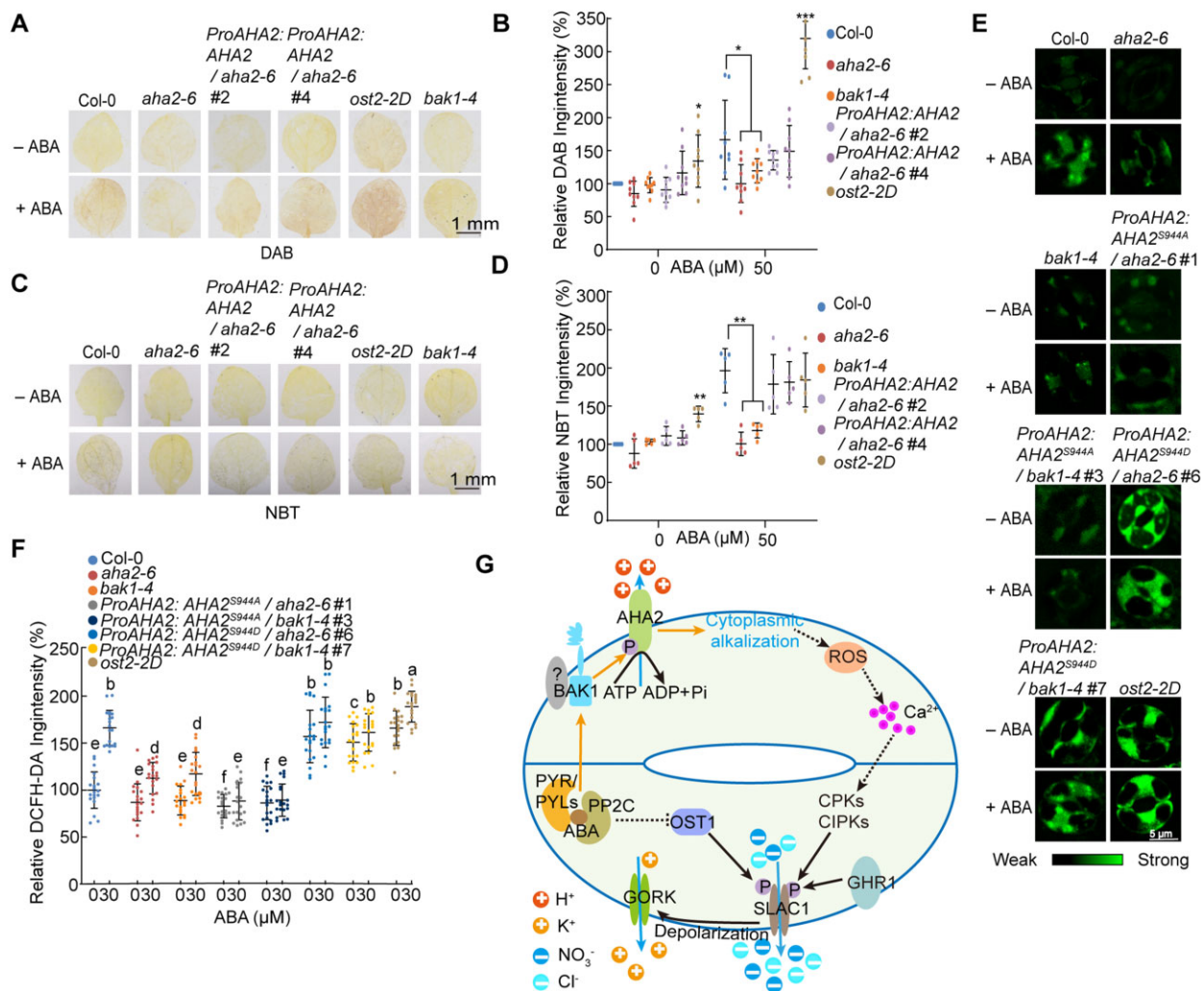


Figure 8 AHA2 and BAK1 are involved in ABA-induced ROS production. A, DAB staining for H_2O_2 in 10-day-old seedlings of Col-0, *aha2-6*, *ProAHA2:AHA2/aha2-6* (lines #2, #4), *ost2-2D*, and *bak1-4* lines treated or not with $50\ \mu\text{M}$ ABA for 5 h. A representative leaf staining pattern is shown. Bar = 1 mm. B, DAB staining intensity, as determined with ImageJ software. Three independent experiments were performed with similar results, each experiment with nine seedlings. Error bars represent SD . Significant difference compared to Col-0 under the same treatment, as determined by Student's *t* test: * $P < 0.05$, *** $P < 0.001$. C, NBT staining for superoxide in 10-day-old seedlings of Col-0, *aha2-6*, *ProAHA2:AHA2/aha2-6* (lines #2, #4), *ost2-2D*, and *bak1-4* lines treated or not with $50\ \mu\text{M}$ ABA for 5 h. A representative leaf staining pattern is shown. Bar = 1 mm. D, NBT staining intensity, as determined with ImageJ software. Three independent experiments were done with similar results, each experiment with five seedlings. Error bars represent SD . Significant difference compared to Col-0 under the same treatment, as determined by Student's *t* test: ** $P < 0.01$. E, Representative images of DCFH-DA fluorescence intensity in guard cells of Col-0, *aha2-6*, *bak1-4*, *ost2-2D*, one transgenic line expressing *ProAHA2:AHA2^{S944D}* in the *aha2-6* or *bak1-4* background and one transgenic line expressing *ProAHA2:AHA2^{S944A}* in the *aha2-6* or *bak1-4* background treated or not with $30\ \mu\text{M}$ ABA for 2 h. Emission = 488 nm. The pseudocolor bar represents the fluorescence intensity (for all panels). Bar = $5\ \mu\text{m}$ (for all panels). F, DCFH-DA fluorescence intensity from 20 guard cells shown in (E). Error bars represent SD . Significant differences represented by different lowercase letters as determined by Student's *t* test ($P < 0.05$). Three independent experiments were performed with similar results. G, Proposed model of BAK1-mediated AHA2 activation during ABA-induced stomatal closure. Under drought stress, ABA activates BAK1, which phosphorylates and activates the PM H^+ -ATPase AHA2, which itself induces cytoplasmic alkalization, produces ROS, and activates Ca^{2+} influx, leading to an increased concentration of cytosolic Ca^{2+} , and finally leads to stomatal closure. The three arrows from ABA to cytoplasmic alkalization represent the main results of this study. The dotted line arrows represent the suspected outcomes. Some known key components in ABA signaling involved in this process were not analyzed in this study. PYR1/PYLs: PYR1/ PYL ABA receptors; PP2C: the clade A protein phosphatase 2C; GORK, Guard cell Outward Rectifying Shaker channel.

plants than in Col-0 plants before ABA treatment, and ROS levels increased in all of these plants after ABA treatment. The ROS levels in *ProAHA2:AHA2^{S944A}/aha2-6* and *ProAHA2:AHA2^{S944A}/bak1-4* plants after ABA treatment

reached a similar level as in Col-0 before ABA treatment (Figure 8, E and F). These results suggest that BAK1 and PM H^+ -ATPases are required for ABA-induced ROS accumulation, with *ost2-2D* constitutively accumulating more ROS.

In guard cells, cytoplasmic alkalinization induced by ABA precedes ROS production, which in turn activates Ca^{2+} channels at the PM (Pei et al., 2000; Murata et al., 2001; Suhita et al., 2004), leading to stomatal closure. Thus, we tested whether PM H^{+} -ATPases and BAK1 act upstream of Ca^{2+} signaling. Exogenous application of Ca^{2+} resulted in stomatal closure to the same degree in Col-0, *bak1-4*, *aha2-6* *bak1-4*, *aha2-4*, and *aha2-6* plants but appeared to have no effect on *ost2-2D* plants, as previously reported (Supplemental Figure S4C) (Merlot et al., 2007). The above results suggest that BAK1 and PM H^{+} -ATPases are involved in mediating ABA-induced elevation in Ca^{2+} levels. Under drought stress, ABA-activated BAK1 phosphorylates and activates AHA2, resulting in a transient H^{+} efflux from the cytoplasm that leads to cytoplasmic alkalinization and ROS production. These accumulated ROS may activate Ca^{2+} channels and finally close stomata (Chen et al., 2021a; Figure 8G).

Discussion

Stomatal closure and opening are typically considered to be regulated by two independent processes: (1) light-induced stomatal opening relies on the activation of PM H^{+} -ATPases that hydrolyze ATP to pump H^{+} from the cytosol to the apoplast, thereby generating a proton electrochemical gradient that drives other cations such as K^{+} into guard cells, partly coupled to H^{+} influx (Wegner and Shabala, 2020; Wegner et al., 2021) and (2) ABA and other factors induce stomatal closure initially by activating SLAC1 and QUAC1 channels to mediate anion efflux and PM depolarization, which activates K^{+} channels for K^{+} efflux (Chen et al., 2020, 2021a). *bak1* mutants are susceptible to drought, with rapid water loss, and their stomatal movement is insensitive to ABA (Shang et al., 2016). However, similar to the role of activated PM H^{+} -ATPases in promoting stomatal opening, we discovered here that activated AHA2 is also required for ABA-induced stomatal closure. Our results suggest that AHA2 is involved in regulating stomatal movement, not because of compensatory transcriptional changes of other AHA genes in the absence of AHA2. Genetic analyses indicate that the loss-of-function mutants *aha2-6* and *bak1-4* and the *aha2-6 bak1-4* double mutant are all similarly insensitive to ABA-mediated stomatal closure. These mutants all suffered from water loss to the same extent (Figure 2). These results suggest that BAK1 works in the same pathway as AHA2 for ABA-induced stomatal closure (Figure 8G).

Cytosolic alkalinization is an early and common event that precedes ROS production during stomatal closure in response to ABA, methyl jasmonate (MeJA) or chitosan (Irving et al., 1992; Suhita et al., 2004; Gonugunta et al., 2009; Islam et al., 2010). During this process, PM H^{+} -ATPases are activated by protein kinase(s), because their activation can be blocked by pretreatment with the common protein kinase inhibitor K252a (Suhita et al., 2004). The

addition of the weak acid butyrate can also reduce ABA- and MeJA-triggered ROS production by lowering cytosolic pH (Suhita et al., 2004). These results suggest that both cytosolic alkalinization and PM H^{+} -ATPases are required for stomatal closure and require protein kinase(s). The rise in cytoplasmic pH induced by ABA was impaired in both *aha2-6* and *bak1-4* mutants, suggesting that both AHA2 and BAK1 are involved in controlling cytoplasmic pH. Consistent with the concept that cytosolic alkalinization precedes ROS production (Irving et al., 1992; Suhita et al., 2004; Gonugunta et al., 2009; Islam et al., 2010), both *aha2-6* and *bak1-4* mutants accumulate less ROS than Col-0, and H_2O_2 treatment induced stomatal closure equally in *aha2-6*, *bak1-4*, and Col-0 plants. A recent study indicated that ABI1 interacts with and inhibits BAK1 (Deng et al., 2022). BAK1 is activated in response to ABA treatment likely through releasing the ABI1 inhibition on BAK1 by ABA-abundant PYLs (Deng et al., 2022). Our results suggest that BAK1 is a key component in the positive regulation of the early signal transduction pathway upstream of PM H^{+} -ATPase-mediated cytoplasmic alkalinization during ABA-induced stomatal closure. Given that BAK1 generally works as a co-receptor, we speculate that other receptor-like protein kinase(s) may cooperate with BAK1 to mediate the activation of PM H^{+} -ATPases (Figure 8G), an idea that needs to be further explored.

We demonstrated here that BAK1 interacts with AHA2 and that the BAK1-KD can phosphorylate and activate AHA2 in vitro. The LRR-RLK PSY1R phosphorylates AHA1 and AHA2 at the Thr-881 residue, which is conserved in all AHA members except AHA10, and activates PM H^{+} -ATPase activity (Niittylä et al., 2007; Rudashevskaya et al., 2012; Fuglsang et al., 2014). However, which protein kinases target the identified phosphorylation sites are not well known (Nühse et al., 2007; Rudashevskaya et al., 2012). Recently, two studies reported that auxin-activated TMK1 and/or TMK4 directly phosphorylate the AHA2 (T947) or AHA1 (T498) penultimate Thr residue and activate these PM H^{+} -ATPases (Li et al., 2021; Lin et al., 2021a). In this study, we determined that AHA2^{S944} can be phosphorylated by BAK1 both in vitro and in vivo. However, Ser-944 is only present in AHA2 and AHA7 (Ser-956; Rudashevskaya et al., 2012). These results suggest that BAK1 regulates AHA2 phosphorylation in ABA-induced stomatal closure. It seems that AHA2 Ser-944 is sufficient for its activation by ABA, as Ser-944-Ala mutation could not, but the phosphorylation mimic form Ser-944-Asp could largely complement the stomatal phenotypes responding to ABA in either *aha2-6* or *bak1-4*. However, we cannot exclude the importance of the other phosphorylation sites of AHA2 by BAK1, and this possibility merits further exploration.

In this study, we observed that H^{+} ions are pumped from the cytosol into the apoplast within 10 min after ABA treatment in Col-0 but not *aha2-6* or *bak1-4* plants, as determined by NMT (Figure 7A), which is similar to previous observations for guard cell responses to MeJA (Munemasa

et al., 2007; Yan et al., 2015). This result contradicts previous reports of the negative regulation of PM H⁺-ATPase activity by ABA (Merlot et al., 2007; Xue et al., 2018). As mentioned above, the biological role of PM H⁺-ATPases is well known for light-induced stomatal opening. We also determined that *aha2* mutants respond normally to inhibition of light-induced stomatal opening by ABA, suggesting that light-induced stomatal opening is not affected by the loss of AHA2. In contrast, the *gpa1* mutation in the G protein α subunit impairs only the inhibition of light-induced stomatal opening by ABA but not ABA-induced stomatal closure, which is independent of pH (Wang et al., 2001), while ABA-induced stomatal closure is dependent on pH in the *aha2-6* mutant. Given that ABA not only activates PM H⁺-ATPases that pump H⁺ into the apoplast to hyperpolarize the PM and activate inwardly rectifying K⁺ channels for K⁺ uptake, but also activates SLAC1 and QUAC1 channels to depolarize the PM and activate outward K⁺ channels for K⁺ efflux, the results obtained in this study are consistent with previous data that mutants in early ABA signaling events such as *abi1-1*, *ost1*, and *ghr1* are impaired in both ABA-induced stomatal closure and inhibition of light-induced stomatal opening by ABA (Leung et al., 1994; Meyer et al., 1994; Mustilli et al., 2002; Hua et al., 2012). However, ABA signaling seems not to be directly involved in inhibiting PM H⁺-ATPases during light-induced stomatal opening as we found in *aha2* mutants in this study. These results indicate that ABA signaling plays dominant roles in promoting stomatal closure during light-induced stomatal opening (Chen et al., 2020, 2021a). The main genetic evidence supporting the possible role of ABA-inhibited PM H⁺-ATPases comes from the gain-of-function mutants *ost2-1/2D*, which have constitutive PM H⁺-ATPase activity (Merlot et al., 2007). However, in this study, we established that *ost2-2D* accumulates more ROS and has a more basic cytoplasmic pH than Col-0. One explanation for the observed resistance of the *ost2-2D* mutant to ABA-induced stomatal closure is likely that this mutant highly hyperpolarizes the PM, which cannot be depolarized by ABA-activated SLAC1 and QUAC1, or other factors such as ROS, and Ca²⁺. Thus, the overly strong phenotypes of *ost2-2D* may mask the real roles of PM H⁺-ATPases in ABA-induced stomatal closure.

ABA-mediated ROS production can occur in different parts of a cell (Qi et al., 2018). A major source of ROS is the PM-localized NADPH oxidases that can be phosphorylated and activated by ABA-activated OST1 (Sirichandra et al., 2009). In the plant disease response, after the bacterial flagellin epitope flag 22 activates the FLS2-BAK1 module, the activated-BAK1 can directly phosphorylate and activate BOTRYTIS-INDUCED KINASE1 (BIK1) kinase that then phosphorylates and activates RbohD to trigger ROS production (Li et al., 2014). ABA can also inhibit the transcription of ABO6/8, two genes encoding proteins involved in regulating splicing of RNAs in mitochondrial complex I, and increase ROS production in mitochondria (He et al., 2012; Yang et al., 2014), or promote ROS production in chloroplasts (Qi

et al., 2018). As we found that ABA can activate BAK1, it is possible that BAK1 promotes ROS production through BIK1 or its homologs PBLs to activate NADPH oxidases. However, the previous studies suggested that ROS production occurs after cytoplasmic alkalinization by ABA (Pei et al., 2000; Murata et al., 2001; Suhita et al., 2004). We also noticed that the *ost2-2D* mutant accumulates more ROS under normal conditions and even further increases ROS levels under ABA treatment compared with the wild-type. Nevertheless, *aha2-6* accumulates less ROS under ABA treatment than the wild-type. Thus, whether pH could trigger ROS production such as through directly influencing the activities of NADPH oxidases, and/or whether pH and the ROS pathway are parallel in ABA signaling, and/or whether BAK1 and OST1 independently regulate NADPH oxidase activity need further study.

In summary, our study provides important evidence for the dual roles of PM H⁺-ATPases not only in light-induced stomatal opening but also in ABA-induced stomatal closure, emphasizing the importance of H⁺ in PM cation and anion influx and efflux (Wegner and Shabala, 2020; Wegner et al., 2021).

Materials and methods

Plant materials and growth conditions

In this study, *A. thaliana* wild-type (Col-0), and the T-DNA insertion lines *bak1-4* (SALK_116202), *aha2-6* (SALK_062371), and *aha2-4* (SALK_082786) were used. The mutant *ost2-2D* was described previously (Merlot et al., 2007). The complementary plants (*ProAHA2:AHA2*; *ProAHA2:AHA2*^{S944A}; *ProAHA2:AHA2*^{S944D}) in *aha2-6* or *bak1-4* and the complementary plants (a Super promoter driving *BAK1-Flag*) in *bak1-4* were generated through *Agrobacterium tumefaciens* GV3101-mediated transformation. All transgenic *A. thaliana* lines and T-DNA insertion mutants used in this study are in the Col-0 ecotype background. The primers used for constructing vectors and identifying these mutants are listed in Supplemental Data Set 1.

The seeds were surface-sterilized in a solution containing 20% (v/v) sodium hypochlorite (NaClO) and 0.1% (v/v) Triton X-100 for 15 min, washed 6 times with sterilized distilled water, sown on MS medium containing 2.5% (w/v) Suc and 0.3% (for horizontal growth) or 0.5% (for vertical growth) Phytagel agar (Sigma-Aldrich, St. Louis, MO, USA), and grown in a growth chamber (22-h light/2-h dark; under LED light with 60 $\mu\text{Em}^{-2} \text{s}^{-1}$ at 23°C) after being kept at 4°C for 3 days in darkness. After 7–10 days, seedlings were planted and grown on soil (16-h light/8-h dark; under LED light with 60 $\mu\text{Em}^{-2} \text{s}^{-1}$ at 20°C \pm 1°C; and 65% relative humidity). For physiological experiments, the seedlings were planted and grown on soil in short-day greenhouse conditions with 12-h white light/12-h dark (under LED light with 60 $\mu\text{Em}^{-2} \text{s}^{-1}$ at 20°C \pm 1°C; and 60% relative humidity).

For the primary root growth assays, 4-day-old seedlings grown on MS medium were transferred to MS medium

supplemented with different concentrations of ABA and vertically cultured for 4 days in a growth chamber.

Split-luciferase complementation assay

The assay was performed as previously described (Chen et al., 2021b). The CDS of *BAK1* was cloned into the 35S promoter driving pCAMBIA1300-nLUC and that of *AHA2* and was cloned into the 35S promoter driving pCAMBIA1300-cLUC. GUS fused with nLUC or cLUC was used as a negative control. The constructs were transformed into *Agrobacterium* GV3101 and co-injected into *N. benthamiana* leaves and cultivated for 48–72 h. The images were captured using a CCD camera (NightSHADE, LB985, Berthold, Germany) after spraying 1 mM of d-luciferin on the leaves. Primer sequences are listed in Supplemental Data Set 1.

Co-IP assay

Co-IP assay was performed as described previously (Kong et al., 2015). The cDNA of Arabidopsis *BAK1* or *SERK4* was cloned into the super promoter driving pCAMBIA1300-Flag, and *AHA2* was cloned into the super promoter driving pCAMBIA1300-MYC. *AHA2*-MYC and *BAK1*-Flag or *SERK4*-Flag were co-transformed into Col-0 protoplasts, respectively. After being cultivated for 16 h under weak light, total proteins were extracted with IP buffer (50 mM Tris-HCl, pH 7.5, 150-mM NaCl, 0.2% Triton X-100, 5-mM dithiothreitol (DTT), 1× PMSF and 1× protease inhibitor cocktail), and then incubated with Myc beads (Sigma-Aldrich) for 2 h. The immunoprecipitated samples were washed 3 times with IP buffer, separated on 8% SDS-PAGE gels and subjected to immunoblot analysis with anti-Myc (dilution of 1:5,000, Cat#HT101-02, TRANSGEN) and anti-Flag antibodies (dilution of 1:5,000; Cat#F3165; Sigma-Aldrich).

Y2H assay

The cDNA of Arabidopsis *BAK1-KD* or *SERK4-KD* was cloned into pGBD7, respectively, and the cDNA of Arabidopsis *AHA2-C₉₉* was cloned into pGADT7. Pair vectors of *BAK1-KD*-BD and *AHA2-C₉₉*-AD, or *SERK4-KD*-BD and *AHA2-C₉₉*-AD, or empty vector pGADT7 and pGBD7 were co-transformed into yeast strain Y2HGold (Clontech, Mountain View, CA, USA), respectively. The yeast cells were grown on –2 SD (–Leu –Trp) or –4 SD (–His –Ade –Leu –Trp) selective medium for 3 days.

Dual membrane system Y2H assay

Vectors of *AHA2*-pPR3-STE, *PKS5*-pBT3-N, *BAK1*-pBT3-SUC, and *GHR1*-pBT3-STE were constructed according to the DUAL membrane system manufacturer's protocols (Clontech, Mountain View, CA, USA), and then co-transformed pairwise into the yeast strain NMY51. Yeast cells were spread on –2 SD (–Leu –Trp) or –3 SD (–His –Leu –Trp) with 3 mM 3 AT selective medium, and cultivated at 30°C for 3 days. *AHA2*-pPR3-STE and *PKS5*-pBT3-N were used as a positive control.

Physiological experiments

All physiological experiments were performed as described previously with some modifications (Hua et al., 2012; Zhu et al., 2020). In the water loss assay of detached leaves, every fifth rosette leaf of 4-week plants grown in a short-day greenhouse conditions (12-h light/12-h dark; under LED light with $60 \mu\text{Em}^{-2} \text{s}^{-1}$ at $20^\circ\text{C} \pm 1^\circ\text{C}$; and 60% relative humidity) was cut and placed on a piece of weighing paper. The rosette leaves were periodically weighed every half hour for 2 h, and every hour for a subsequent 4 h. Water loss was shown as a percentage of the original fresh weight. At least three independent experiments were performed.

For the drought assay on soil, every nine 7-day-old seedlings were transferred onto one pot filled with an equal amount of soil, and grown for another 7 days in short-day greenhouse conditions (12-h light/12-h dark; under LED light with $60 \mu\text{Em}^{-2} \text{s}^{-1}$ at $20^\circ\text{C} \pm 1^\circ\text{C}$; and 60% relative humidity). After the soil in each pot had fully absorbed water, pots were put on a rotating plate board with one round per 80 s so that each plant was uniformly illuminated, and water was withheld from these pots for about 16 days. The plants were photographed when the soil moisture was reduced to 58%–55%. Photographs were taken 3 days after fully and equally rewatering the plants.

The water loss assay on soil was performed as described previously (Hua et al., 2012). Every five seedlings of one pot were grown for 4 weeks under short-day greenhouse conditions (12-h light/12-h dark; under LED light with $60 \mu\text{Em}^{-2} \text{s}^{-1}$ at $20^\circ\text{C} \pm 1^\circ\text{C}$; and 60% relative humidity). The water loss of plants growing on soil was measured by weighing each pot with an electronic balance every 5 min for 3 days. The data were recorded by a computer that was connected to the balance. The data from three individual pots for 1 day were analyzed.

For the stomatal aperture or number assays, epidermal strips were peeled from the fourth rosette leaf of a 4-week-old plant in soil, and then incubated in MES buffer (10-mM MES-KOH, pH 6.15, 10-mM KCl, and 50- μM CaCl_2) in an illumination incubator (22-h light/2-h dark; under LED light with $60 \mu\text{Em}^{-2} \text{s}^{-1}$ at 23°C) for 4 h to ensure that the stomata were fully opened. The epidermal strips were transferred to MES buffer containing 10- μM ABA, 0.2-mM H_2O_2 , or 0.5-mM CaCl_2 , respectively, for 2 h at 23°C . To study the inhibition of light-induced stomatal opening by ABA, the plants were put in darkness for 24 h to close the stomata before epidermal strips were peeled and incubated with MES buffer containing 10- μM ABA for 2 h in an illumination incubator (22-h light/2-h dark; under LED light with $60 \mu\text{Em}^{-2} \text{s}^{-1}$ at 23°C). The stomatal aperture or stomatal number were examined double-blind under a $40\times$ objective with a light microscope and measured using ImageJ software.

For the Infrared thermal imaging assay, every nine 10-day soil-grown seedlings in one pot under short-day greenhouse conditions (12-h light/12-h dark; under LED light with $60 \mu\text{Em}^{-2} \text{s}^{-1}$ at $20^\circ\text{C} \pm 1^\circ\text{C}$; and 60% relative humidity), were photographed using an Infrared thermal imager when soil moisture was 80%–75%.

Stomatal conductance in response to the ABA or O₃ was determined as described previously (Kollist et al., 2007). A 3- to 4-week-old whole plant in a pot was used for sustaining recording stomatal conductance for 30 min. Then the stimulus (5- μ M ABA or 400 ppb O₃ for 5 min) was applied and stomatal conductance was recorded for another 70 min.

For recording photosynthetic rate, a previously described method was used (Wang and Kinoshita, 2017). The soil-grown whole plants were grown in short-day greenhouse conditions (12-h light/12-h dark; under LED light with 60 μ Em⁻² s⁻¹ at 21°C \pm 1°C; and 60% relative humidity) for 14 days. The first measurement by the LI-6400XT photosynthesis measuring system (Licor, USA) was performed when the soil moisture was 95%–90%. After withholding water until the soil moisture reached 80%–75%, the second measurement was taken for the same plants.

Kinase activity assay

The CDS of *BAK1-KD* was cloned into the pET28a vector and the CDS of *AHA2-C₉₉* was cloned into the pGEX-4T-1 vector. Recombinant proteins HIS-BAK1-KD and GST-AHA2-C₉₉ and the mutant proteins of GST-AHA2-C₉₉ (T858A, T881A, S944A, Y946A, T858A/S944A/Y946A, and T881A/T858A/S944A/Y946A) were purified from BL21 *E. coli* and subjected to an in vitro phosphorylation assay. About 3- μ g HIS-BAK1-KD, 2 μ g GST-AHA2-C₉₉, and the mutant proteins were incubated in kinase buffer (2-mM Tris-HCl, pH 7.5, 1- μ M CaCl₂, 0.2-mM DTT, 0.5-mM MgCl₂, 0.1-mM MnCl₂) with 50- μ M cold ATP and 1 μ Ci [γ -³²P] ATP at 30°C for 30 min. Proteins were separated by 10% SDS-PAGE. After Coomassie blue staining, the radioactivity was detected using a Typhoon 9410 imager (Amersham, USA).

For the in vitro phosphorylation assay from plants, total proteins were isolated with IP buffer from the *bak1-4* and *bak1-4* complemented seedlings (Super promoter driving *BAK1:BAK1-Flag/bak1-4*) treated with 50- μ M ABA for 30 min, and immunoprecipitated with Flag-beads (Sigma-Aldrich). Then the immunoprecipitated proteins were incubated with 2- μ g GST-AHA2-C₉₉ protein in kinase buffer with 50- μ M cold ATP and 1- μ Ci [γ -³²P] ATP at 30°C for 30 min, and separated by 10% SDS-PAGE. After Coomassie blue staining, the gels were put into the phosphor screen. Finally, radioactivity was detected using a Typhoon 9410 imager. The proteins from *bak1-4* seedlings were used as a negative control.

For the in vivo phosphorylation assay from plants, 10-day-old Col-0, *bak1-4*, or *aha2-6* seedlings were treated with 50- μ M ABA or 1/2 MS for 30 min before total PM proteins were isolated. The PM isolation assay was performed as described previously (Qiu et al., 2002; Yang et al., 2010) with some modifications. About 1 g of seedlings was ground with liquid nitrogen and suspended in isolation buffer (0.33 M Suc, 0.2% [w/v] bovine serum albumin, 10% [w/v] glycerol, 5-mM DTT, 5-mM EDTA, 5-mM ascorbate, 0.6% [w/v] polyvinylpyrrolidone, 0.2% [w/v] casein, 1-mM phenylmethylsulfonyl fluoride, and 50-mM HEPES-KOH, pH 7.5). The homogenate was centrifuged at 10,000g for 10 min, and

then the supernatant was filtered through two layers of Miracloth. Subsequently, the sediment was obtained by centrifugation for 1 h at 100,000g from the supernatant. The sediment was then resuspended in buffer I (0.33-M Suc, 3-mM KCl, 1-mM DTT, 1-mM phenylmethylsulfonyl fluoride, 2-mM EDTA, 5-mM K⁺ phosphate with pH 7.8, and 1 \times protease inhibitor, pH 7.5). The PM (upper phase) was obtained using precold two-phase mixture (6.2% [w/w] Dextran T-500, 0.33 M Suc, 0.1-mM EDTA, 1-mM DTT, 6.2% [w/w] polyethylene glycol 3350, and 5-mM K⁺ phosphate with pH 7.8) by standing on the ice 15 min or centrifuging the tubes at 1,000g for 5 min. Buffer II (0.33-M Suc, 2-mM DTT, 0.1-mM EDTA, 1-mM phenylmethylsulfonyl fluoride, 20-mM HEPES-KOH, and 1 \times protease inhibitor, pH 7.5) was added to dilute the PMs, and samples were then centrifuged for 1 h at 100,000g. The sediment was resuspended with buffer II containing 1-mM EDTA to obtain the PM. The PM proteins were divided in half and separated by 8% SDS-PAGE. One half was subjected to immunoblot analysis with anti-AHA2^{S944} (BPI, China) antibodies and the other was subjected to immunoblot analysis with anti-ATPase (dilution of 1:2,000, Cat#AS07260, Agrisera) antibodies as the loading control. The synthetic peptide CKGHVESVVKL with S phosphorylation was used for making anti-AHA2^{S944} antibodies in rabbits (dilution of 1:500, BPI, China).

HIS-BAK1-KD (3 μ g) and GST-AHA2-C₉₉ (2 μ g) recombinant proteins purified from *E. coli* were incubated in kinase buffer (2-mM Tris-HCl, pH 7.5, 11 μ M CaCl₂, 0.2-mM DTT, 0.5-mM MgCl₂, 0.1mM MnCl₂) with 50- μ M cold ATP at 30°C for 30 min. The proteins were divided in half, and separated by 10% SDS-PAGE. One half was for Coomassie blue staining and the other was subjected to immunoblot analysis with anti-AHA2^{S944} (BPI, China) antibody.

PM H⁺-ATPase activity assays

Four-week-old Arabidopsis plants grown under short-day greenhouse conditions (12-h light/12-h dark; under LED light with 60 μ Em⁻² s⁻¹ at 21°C \pm 1°C; and 60% relative humidity) were treated with 250-mM NaCl for 3 days. About 50 g rosette leaves were cut and ground with liquid nitrogen for the PM isolation assay as described above. The isolated PM vesicles were used to measure H⁺-transport activity. The H⁺-transport activity of PM H⁺-ATPase was measured as described previously (Qiu et al., 2002; Yang et al., 2010). The H⁺ produced by PM H⁺-ATPase formed an inside-acid pH gradient (Δ pH) in the vesicles, and it was measured as a decrease (quench) in the fluorescence by a pH-sensitive fluorescence probe (quinacrine).

Fifty nanograms of PM vesicles from wild-type plants were incubated with 10 μ g of BAK1-KD protein at 25°C for 30 min, and then 1-mL measurement buffer (3-mM MgSO₄, 100-mM KCl, and 25-mM 1, 3-Bis [Tris (hydroxymethyl) methylamino] propane-HEPES, 250-mM mannitol, and 5-mM quinacrine, pH 6.5) was added to the mixtures. The samples were then transferred into a cuvette and placed in a fluorescence spectrophotometer (Hitachi F-7000) with 430-nm excitation and 500 nm emission wavelength. After the mixtures

were stirred in the dark for 2 min, fluorescence was recorded for 5 min with the addition of the final concentration of 3-mM ATP. About 20-mM Carbonyl cyanide *m*-chlorophenyl hydrazone (a protonophore) was supplied to dissipate the remaining pH gradient and stop the reaction.

Measurement of net fluxes of H⁺ in guard cells

Net fluxes of H⁺ were measured using NMT as described (Yan et al., 2015). A change of hydrogen ion flow rate near guard cells detected by NMT is thought to indicate the activity of PM H⁺-ATPase (Yan et al., 2015). The H⁺-microsensor was prepared as follows: A backfilling solution (40-mM KH₂PO₄ and 15-mM NaCl, pH 7.0) was first filled into a prepulled and silanized microsensor (Φ1.5±0.5 μm, XY-CGQ-02, YoungerUSA) by an injector with a length of 10 mm. The tip of the microsensor was filled selective liquid ion-exchange cocktails (H⁺ LIX, XY-SJ-H, YoungerUSA) to a length of 40 μm under the microscope. The microsensor was connected to an Ag/AgCl wire microsensor holder (YG003-Y11, used as the reference microsensor, YoungerUSA) to make electrical contact with the electrolyte solution. The reference microsensor was balanced in 5 mL of guard cell measuring buffer (0.2-mM Na₂SO₄, 0.1-mM CaCl₂, 0.1-mM MgCl₂, 0.1-mM KCl, 0.5-mM NaCl and 0.3-mM MES, pH 6.5) for 30 min before being calibrated in calibrating buffer (0.1-mM CaCl₂, 0.1-mM KCl, and 0.3-mM MES), with different concentrations of H⁺: pH 5.55 and pH 6.5, respectively. Only a microsensor with a Nernstian slope >50 mV/decade was used in this study. The same microsensors were calibrated again according to the same procedure and standards after each test.

For the measurement steps, the epidermal strip was peeled from the fourth rosette leaf of a 4-week-old plant, and was incubated in 5-mL guard cell measuring buffer for 45 min. Replaced a new 5 mL of the guard cell measuring buffer into the cultural media and putted the cultural media into the control console under the microscope. Before measurements were taken, the distance between the calibrated microsensor and the guard cell was adjusted under the microscope until the calibrated microsensor was ~5–10 mm above the guard cells. A phase-sensitive operational amplifier was used to obtain real-time (~6 s) measurements of transmembrane H⁺ flux. Measurements were taken continuously for 3 min. Then, 30-μM ABA was added and measurements were continued for 9 min and stopped finally. The effect of ABA on H⁺ flux in guard cells was calculated based on the proton flow rate.

Measurement of cytosolic pH

Changes in cytosolic pH in guard cells were measured via confocal microscopy using the pH-sensitive dye SNARF-1-AM (Zhang et al., 2001). Epidermal strips were peeled from the fourth rosette leaf of a 4-week-old plant, and then incubated in MES buffer (10-mM MES-KOH, pH 6.15, 10-mM KCl, and 50-μM CaCl₂) in an illumination incubator for 4 h to ensure the stomata were fully opened. After this incubation, 20-μM SNARF-1-AM was added from a 3-mM stock

solution in DMSO, along with 0.05% pluronic F-127, and samples were incubated for 30 min in the dark at 25°C–27°C. For ABA treatment, the seedlings were incubated with 10-μM ABA for 10 min. Samples were then washed several times with the incubation buffer to clear excess dye prior to imaging. Dye-loaded guard cells were examined using a laser-scanning confocal microscope (Bio-Rad MicroRadiance) with the following wavelength settings: Excitation = 488 nm; Emission = 580 nm (channel 1) and Emission > 600 nm (channel 2). The Nikon TE300 inverted microscope (objective 40/0.60 Plan Fluor) was used for image analyses. Signals from selected frames were scanned simultaneously in both channels and the intensity ratio (channel 1: channel 2) was calculated for each pixel. Each data point was obtained from at least 20 guard cells.

To convert the measured intensity ratios to pH, a ratio-versus-pH curve calibration graph was obtained as follows: SNARF-preloaded epidermal strips were incubated in MES buffers, pH 5.5–7.5 (adjusted with Tris), containing 50-mM KCl, 10-mM MES, 10-mM nigericin (a K⁺/H⁺ exchanger, which equilibrates the external and internal pH), for another 20 min. Fluorescence ratios were obtained by scanning guard cells of defined pH values. Changes in intracellular pH can be calculated as a linear relationship between pH and fluorescence intensity ratios over the pH ranges 5.5–7.5.

ROS measurement in plants

ROS was measured in seedlings as described previously (Yang et al., 2014) with some modifications. Ten-day-old seedlings were treated in liquid MS with or without 50-μM ABA for 5 h. For DAB staining to detect H₂O₂, the seedlings were incubated in 0.3 mg/mL DAB (Sigma-Aldrich) dissolved in 50-mM Tris-HCl (pH 5.0) for 8 h. For NBT staining to detect superoxides, the seedlings were incubated in an NBT (Sigma-Aldrich) reaction buffer (1-mM NBT, 20-mM K-phosphate, 0.1-M NaCl, pH 6.2) for 15 min. Dye-loaded seedlings were then washed 3 times with water. The seedlings were incubated in acidified methanol buffer (10-mL methanol, 2-mL HCl, 38-mL ddH₂O) at 57°C for 15 min (until transparent), and then soaked in a basic solution containing 7% NaOH in 60% ethanol for 15 min at room temperature. The seedlings were incubated 10 min at each step in the following series: 40% ethanol, 20% ethanol, 10% ethanol, 5% ethanol, and 25% glycerol, and finally were examined in 50% glycerol with an Olympus BX53 microscope.

For the DCFH-DA (2', 7'-dichlorodihydrofluorescein diacetate) assay, epidermal strips were peeled from the rosette leaves of 4-week-old plants, and then incubated in MES buffer (10-mM MES-KOH, pH 6.15, 10-mM KCl, and 50-μM CaCl₂) in an illumination incubator for 4 h to ensure the stomata were fully opened. After this incubation, 50-μM DCFH-DA was added from a 0.5-mM stock solution in KPHO₄ (pH 6.0), and the samples were incubated for 30 min in the dark at 25°C–27°C. For ABA treatment, the seedlings were incubated in MES buffer for 4 h and with 30-μM ABA for 2 h before being incubated with DCFH-DA. Samples were then washed several times with the incubation buffer to

clear excess dye prior to imaging. Dye-loaded guard cells were examined using a laser-scanning confocal microscope (Bio-Rad MicroRadiance) with the following wavelength settings: Excitation = 488 nm; Emission = 505–530 nm. The Nikon TE300 inverted microscope (objective 40/0.60 Plan Fluor) was used for image analyses. Each data point was obtained from 20 guard cells.

RT-qPCR

Total RNAs of 10-day-old seedlings were extracted using a HiPure Plant RNA Mini Kit (Magen, R4151). First-strand cDNA synthesis of 4 µg RNAs was performed using a Maxima H Minus First Strand cDNA Synthesis Kit (Thermo Scientific, K1682). RT-qPCR was performed using a StepOne Plus PCR system with SYBR Green Mix (TaKaRa, Shiga, Japan). The primers used for RT-qPCR are listed in [Supplemental Data Set 1](#).

Statistical analysis

All statistical analyses were performed by using two-tailed Student's *t* tests in Microsoft Excel. Different letters represent statistical significance, while the same letters mean no significant difference. The statistical results are shown in [Supplemental Data Set 2](#).

Accession numbers

Sequence data in this article can be found in The Arabidopsis Information Resource under the following accession numbers: *AHA2* (AT4G30190), *BAK1* (AT4G33430), *SERK4* (AT2G13790), *PKS5* (AT2G30360), and *GHR1* (AT4G20940).

Supplemental data

The following materials are available in the online version of this article.

Supplemental Figure S1. Genetic analysis of *aha2* mutants.

Supplemental Figure S2. Genetic analysis of *aha2-6* complemented with ProAHA2:AHA2.

Supplemental Figure S3. AHA2 do not function in ABA-mediated inhibition in root growth and seed germination.

Supplemental Figure S4. BAK1 and AHA2 act upstream of ROS and Ca²⁺ in ABA-induced stomatal closure.

Supplemental Table S1. Reagents and resources used in this study.

Supplemental Data Set 1. Primers used in this study.

Supplemental Data Set 2. Statistical analyses for different figures.

Funding

This research is supported by grants from the National Science Foundation of China (31730007 and 31921001).

Conflict of interest statement. None declared.

References

- Ando E, Kinoshita T (2018) Red light-induced phosphorylation of plasma membrane H⁺-ATPase in stomatal guard cells. *Plant Physiol* **178**: 838–849
- Blatt MR (1992) K⁺ channels of stomatal guard cells. Characteristics of the inward rectifier and its control by pH. *J Gen Physiol* **99**: 615–644
- Chang YN, Zhu C, Jiang J, Zhang HM, Zhu JK, Duan CG (2020) Epigenetic regulation in plant abiotic stress responses. *J Integr Plant Biol* **62**: 563–580
- Chen K, Li GJ, Bressan RA, Song CP, Zhu JK, Zhao Y (2020) Abscisic acid dynamics, signaling, and functions in plants. *J Integr Plant Biol* **62**: 25–54
- Chen XX, Ding YL, Yang YQ, Song CP, Wang BS, Yang SH, Guo Y, Gong ZZ (2021a) Protein kinases in plant responses to drought, salt, and cold stress. *J Integr Plant Biol* **63**: 53–78
- Chen XX, Wang TT, Rehman AU, Wang Y, Qi JS, Li Z, Song CP, Wang BS, Yang SH, Gong ZZ (2021b) Arabidopsis U-box E3 ubiquitin ligase PUB11 negatively regulates drought tolerance by degrading the receptor-like protein kinases LRR1 and KIN7. *J Integr Plant Biol* **63**: 494–509
- Deng JP, Kong LY, Zhu YH, Pei D, Chen XX, Wang Y, Qi JS, Song CP, Yang SH, Gong ZZ (2022) BAK1 plays contrasting roles in regulating abscisic acid-induced stomatal closure and abscisic acid-inhibited primary root growth in Arabidopsis. *J Integr Plant Biol* <https://doi.org/10.1111/jipb.13257>
- Dong H, Bai L, Zhang Y, Zhang GZ, Mao YQ, Min LL, Xiang FY, Qian DD, Zhu XH, Song CP (2018) Modulation of guard cell turgor and drought tolerance by a peroxisomal acetate-malate shunt. *Mol Plant* **11**: 1278–1291
- Duby G, Poreba W, Piotrowiak D, Bobik K, Derua R, Waelkens E, Boutry M (2009) Activation of plant plasma membrane H⁺-ATPase by 14-3-3 proteins is negatively controlled by two phosphorylation sites within the H⁺-ATPase C-terminal region. *J Biol Chem* **284**: 4213–4221
- Fabregas N, Yoshida T, Fernie AR (2020) Role of Raf-like kinases in SnRK2 activation and osmotic stress response in plants. *Nat Commun* **11**: 6184
- Falhof J, Pedersen JT, Fuglsang AT, Palmgren M (2016) Plasma membrane H⁽⁺⁾-ATPase regulation in the center of plant physiology. *Mol Plant* **9**: 323–337
- Flutsch S, Wang YZ, Takemiya A, Vialet-Chabrand SRM, Klejchova M, Nigro A, Hills A, Lawson T, Blatt MR, Santelia D (2020) Guard cell starch degradation yields glucose for rapid stomatal opening in Arabidopsis. *Plant Cell* **32**: 2325–2344
- Fuglsang AT, Borch J, Bych K, Jahn TP, Roepstorff P, Palmgren MG (2003) The binding site for regulatory 14-3-3 protein in plant plasma membrane H⁺-ATPase: involvement of a region promoting phosphorylation-independent interaction in addition to the phosphorylation-dependent C-terminal end. *J Biol Chem* **278**: 42266–42272
- Fuglsang AT, Guo Y, Cuin TA, Qiu Q, Song C, Kristiansen KA, Bych K, Schulz A, Shabala S, Schumaker KS, et al (2007) Arabidopsis protein kinase PKS5 inhibits the plasma membrane H⁺-ATPase by preventing interaction with 14-3-3 protein. *Plant Cell* **19**: 1617–1634
- Fuglsang AT, Kristensen A, Cuin TA, Schulze WX, Persson J, Thuesen KH, Ytting CK, Oehlenschlaeger CB, Mahmood K, Sondergaard TE, et al (2014) Receptor kinase-mediated control of primary active proton pumping at the plasma membrane. *Plant J* **80**: 951–964
- Fuglsang AT, Paez-Valencia J, Gaxiola RA (2011) Plant proton pumps: regulatory circuits involving H⁺-ATPase and H⁺-PPase. *Transporters and Pumps in Plant Signaling*. Springer Science & Business Media, Berlin, Germany, pp 39–64
- Gaxiola RA, Palmgren MG, Schumacher K (2007) Plant proton pumps. *FEBS Lett* **581**: 2204–2214

- Geiger D, Scherzer S, Mumm P, Stange A, Marten I, Bauer H, Ache P, Matschi S, Liese A, Al-Rasheid KA, et al (2009) Activity of guard cell anion channel SLAC1 is controlled by drought-stress signaling kinase-phosphatase pair. *Proc Natl Acad Sci USA* **106**: 21425–21430
- Gonugunta VK, Srivastava N, Puli MR, Raghavendra AS (2008) Nitric oxide production occurs after cytosolic alkalinization during stomatal closure induced by abscisic acid. *Plant Cell Environ* **31**: 1717–1724
- Gonugunta VK, Srivastava N, Raghavendra AS (2009) Cytosolic alkalinization is a common and early messenger preceding the production of ROS and NO during stomatal closure by variable signals, including abscisic acid, methyl jasmonate and chitosan. *Plant Signal Behav* **4**: 561–564
- Grabov A, Blatt MR (1998) Membrane voltage initiates Ca^{2+} waves and potentiates Ca^{2+} increases with abscisic acid in stomatal guard cells. *Proc Natl Acad Sci USA* **95**: 4778–4783
- Han JP, Koster P, Drerup MM, Scholz M, Li SZ, Edel KH, Hashimoto K, Kuchitsu K, Hippler M, Kudla J (2019) Fine-tuning of RBOHF activity is achieved by differential phosphorylation and Ca^{2+} binding. *New Phytol* **221**: 1935–1949
- Haruta M, Burch HL, Nelson RB, Barrett-Wilt G, Kline KG, Mohsin SB, Young JC, Otegui MS, Sussman MR (2010) Molecular characterization of mutant Arabidopsis plants with reduced plasma membrane proton pump activity. *J Biol Chem* **285**: 17918–17929
- Haruta M, Sabat G, Stecker K, Minkoff BB, Sussman MR (2014) A peptide hormone and its receptor protein kinase regulate plant cell expansion. *Science* **343**: 408–411
- Hayashi Y, Nakamura S, Takemiya A, Takahashi Y, Shimazaki K, Kinoshita T (2010) Biochemical characterization of in vitro phosphorylation and dephosphorylation of the plasma membrane H^+ -ATPase. *Plant Cell Physiol* **51**: 1186–1196
- He JN, Duan Y, Hua DP, Fan GJ, Wang L, Liu Y, Chen ZZ, Han LH, Qu LJ, Gong ZZ (2012) DEXH box RNA helicase-mediated mitochondrial reactive oxygen species production in Arabidopsis mediates crosstalk between abscisic acid and auxin signaling. *Plant Cell* **24**: 1815–1833
- Hiyama A, Takemiya A, Munemasa S, Okuma E, Sugiyama N, Tada Y, Murata Y, Shimazaki K (2017) Blue light and CO_2 signals converge to regulate light-induced stomatal opening. *Nat Commun* **8**: 1284
- Horak H, Sierla M, Toldsepp K, Wang C, Wang YS, Nuhkat M, Valk E, Pechter P, Merilo E, Salojarvi J, et al (2016) A dominant mutation in the HT1 kinase uncovers roles of MAP kinases and GHR1 in CO_2 -induced stomatal closure. *Plant Cell* **28**: 2493–2509
- Hua D, Wang C, He J, Liao H, Duan Y, Zhu Z, Guo Y, Chen Z, Gong Z (2012) A plasma membrane receptor kinase, GHR1, mediates abscisic acid- and hydrogen peroxide-regulated stomatal movement in Arabidopsis. *Plant Cell* **24**: 2546–2561
- Imes D, Mumm P, Böhm J, Al-Rasheid KA, Marten I, Geiger D, Hedrich R (2013) Open stomata 1 (OST1) kinase controls R-type anion channel QUAC1 in Arabidopsis guard cells. *Plant J* **74**: 372–382
- Inoue S, Kinoshita T, Matsumoto M, Nakayama KI, Doi M, Shimazaki K (2008) Blue light-induced autophosphorylation of phototropin is a primary step for signaling. *Proc Natl Acad Sci USA* **105**: 5626–5631
- Irving HR, Gehring CA, Parish RW (1992) Changes in cytosolic pH and calcium of guard cells precede stomatal movements. *Proc Natl Acad Sci USA* **89**: 1790–1794
- Islam MM, Hossain MA, Jannat R, Munemasa S, Nakamura Y, Mori IC, Murata Y (2010) Cytosolic alkalinization and cytosolic calcium oscillation in Arabidopsis guard cells response to ABA and MeJA. *Plant Cell Physiol* **51**: 1721–1730
- Katsuta S, Masuda G, Bak H, Shinozawa A, Kamiyama Y, Umezawa T, Takezawa D, Yotsui I, Taji T, Sakata Y (2020) Arabidopsis Raf-like kinases act as positive regulators of subclass III SnRK2 in osmotic stress signaling. *Plant J* **103**: 634–644
- Kemmerling B, Schwedt A, Rodriguez P, Mazzotta S, Frank M, Qamar SA, Mengiste T, Betsuyaku S, Parker JE, Mussig C, et al (2007) The BRI1-associated kinase 1, BAK1, has a brassinolide-independent role in plant cell-death control. *Curr Biol* **17**: 1116–1122
- Kim TH, Böhmer M, Hu H, Nishimura N, Schroeder JI (2010) Guard cell signal transduction network: advances in understanding abscisic acid, CO_2 , and Ca^{2+} signaling. *Annu Rev Plant Biol* **61**: 561–591
- Kinoshita T, Doi M, Suetsugu N, Kagawa T, Wada M, Shimazaki K (2001) Phot1 and phot2 mediate blue light regulation of stomatal opening. *Nature* **414**: 656–660
- Kinoshita T, Shimazaki K (1999) Blue light activates the plasma membrane H^+ -ATPase by phosphorylation of the C-terminus in stomatal guard cells. *EMBO J* **18**: 5548–5558
- Kollist T, Moldau H, Rasulov B, Oja V, Ramma H, Huve K, Jaspers P, Kangasjarvi J, Kollist H (2007) A novel device detects a rapid ozone-induced transient stomatal closure in intact Arabidopsis and its absence in *abi2* mutant. *Physiol Plant* **129**: 796–803
- Kong LY, Cheng JK, Zhu YJ, Ding YL, Meng JJ, Chen ZZ, Xie Q, Guo Y, Li JG, Yang SH, et al (2015) Degradation of the ABA co-receptor ABI1 by PUB12/13 U-box E3 ligases. *Nat Commun* **6**: 8630
- Leung J, Bouvier-Durand M, Morris PC, Guerrier D, Cheddor F, Giraudat J (1994) Arabidopsis ABA response gene ABI1: features of a calcium-modulated protein phosphatase. *Science* **264**: 1448–1452
- Li J, Wen J, Lease KA, Doke JT, Tax FE, Walker JC (2002) BAK1, an Arabidopsis LRR receptor-like protein kinase, interacts with BRI1 and modulates brassinosteroid signaling. *Cell* **110**: 213–222
- Li L, Li M, Yu LP, Zhou ZY, Liang XX, Liu ZX, Cai GH, Gao LY, Zhang XJ, Wang YC, et al (2014) The FLS2-associated kinase BIK1 directly phosphorylates the NADPH oxidase RbohD to control plant immunity. *Cell Host Microbe* **15**: 329–338
- Li LX, Verstraeten I, Roosjen I, Takahashi K, Rodriguez L, Merrin J, Chen J, Shabala L, Smet W, Ren H, et al (2021) Cell surface and intracellular auxin signalling for H^+ fluxes in root growth. *Nature* **599**: 273
- Lin WW, Zhou X, Tang WX, Takahashi K, Pan X, Dai JW, Ren H, Zhu XY, Pan SQ, Zheng HY, et al (2021a) TMK-based cell-surface auxin signalling activates cell-wall acidification. *Nature* **599**: 278
- Lin Z, Li Y, Wang YB, Liu XL, Ma L, Zhang ZJ, Mu C, Zhang Y, Peng L, Xie SJ, et al (2021b) Initiation and amplification of SnRK2 activation in abscisic acid signaling. *Nat Commun* **12**: 2456
- Lin Z, Li Y, Zhang ZJ, Liu XL, Hsu CC, Du YY, Sang T, Zhu C, Wang YB, Satheesh V, et al (2020) A RAF-SnRK2 kinase cascade mediates early osmotic stress signaling in higher plants. *Nat Commun* **11**: 613
- Ma Y, Szostkiewicz I, Korte A, Moes D, Yang Y, Christmann A, Grill E (2009) Regulators of PP2C phosphatase activity function as abscisic acid sensors. *Science* **324**: 1064–1068
- Mao J, Zhang YC, Sang Y, Li QH, Yang HQ (2005) A role for Arabidopsis cryptochromes and COP1 in the regulation of stomatal opening. *Proc Natl Acad Sci USA* **102**: 12270–12275
- Merlot S, Leonhardt N, Fenzi F, Valon C, Costa M, Piette L, Vavasseur A, Genty B, Boivin K, Muller A, et al (2007) Constitutive activation of a plasma membrane H^+ -ATPase prevents abscisic acid-mediated stomatal closure. *EMBO J* **26**: 3216–3226
- Meyer K, Leube MP, Grill E (1994) A protein phosphatase 2C involved in ABA signal transduction in *Arabidopsis thaliana*. *Science* **264**: 1452–1455
- Meyer S, Mumm P, Imes D, Endler A, Weder B, Al-Rasheid KA, Geiger D, Marten I, Martinoia E, Hedrich R (2010) AtALMT12 represents an R-type anion channel required for stomatal movement in Arabidopsis guard cells. *Plant J* **63**: 1054–1062
- Miao R, Yuan W, Wang Y, Garcia-Maquilon I, Dang XL, Li Y, Zhang JH, Zhu YY, Rodriguez PL, Xu WF (2021) Low ABA

- concentration promotes root growth and hydrotropism through relief of ABA INSENSITIVE 1-mediated inhibition of plasma membrane H^+ -ATPase 2. *Sci Adv* **7**: eabd4113
- Munemasa S, Oda K, Watanabe-Sugimoto M, Nakamura Y, Shimoishi Y, Murata Y** (2007) The coronatine-insensitive 1 mutation reveals the hormonal signaling interaction between abscisic acid and methyl jasmonate in Arabidopsis guard cells. Specific impairment of ion channel activation and second messenger production. *Plant Physiol* **143**: 1398–1407
- Murata Y, Pei ZM, Mori IC, Schroeder J** (2001) Abscisic acid activation of plasma membrane Ca^{2+} channels in guard cells requires cytosolic NAD(P)H and is differentially disrupted upstream and downstream of reactive oxygen species production in *abi1-1* and *abi2-1* protein phosphatase 2C mutants. *Plant Cell* **13**: 2513–2523
- Mustilli AC, Merlot S, Vavasseur A, Fenzi F, Giraudat J** (2002) Arabidopsis OST1 protein kinase mediates the regulation of stomatal aperture by abscisic acid and acts upstream of reactive oxygen species production. *Plant Cell* **14**: 3089–3099
- Nam KH, Li J** (2002) BRI1/BAK1, a receptor kinase pair mediating brassinosteroid signaling. *Cell* **110**: 203–212
- Niittylä T, Fuglsang AT, Palmgren MG, Frommer WB, Schulze WX** (2007) Temporal analysis of sucrose-induced phosphorylation changes in plasma membrane proteins of Arabidopsis. *Mol Cell Proteomics* **6**: 1711–1726
- Nühse TS, Bottrill AR, Jones AM, Peck SC** (2007) Quantitative phosphoproteomic analysis of plasma membrane proteins reveals regulatory mechanisms of plant innate immune responses. *Plant J* **51**: 931–940
- Palmgren MG** (2001) PLANT PLASMA MEMBRANE H^+ -ATPases: powerhouses for nutrient uptake. *Annu Rev Plant Physiol Plant Mol Biol* **52**: 817–845
- Palmgren MG, Axelsen KB** (1998) Evolution of P-type ATPases. *Biochim Biophys Acta* **1365**: 37–45
- Palmgren MG, Larsson C, Sommarin M** (1990) Proteolytic activation of the plant plasma membrane H^+ -ATPase by removal of a terminal segment. *J Biol Chem* **265**: 13423–13426
- Pandey S, Zhang W, Assmann SM** (2007) Roles of ion channels and transporters in guard cell signal transduction. *FEBS Lett* **581**: 2325–2336
- Park SY, Fung P, Nishimura N, Jensen DR, Fujii H, Zhao Y, Lumba S, Santiago J, Rodrigues A, Chow TF, et al** (2009) Abscisic acid inhibits type 2C protein phosphatases via the PYR/PYL family of START proteins. *Science* **324**: 1068–1071
- Pei ZM, Murata Y, Benning G, Thomine S, Klüsener B, Allen GJ, Grill E, Schroeder JI** (2000) Calcium channels activated by hydrogen peroxide mediate abscisic acid signalling in guard cells. *Nature* **406**: 731–734
- Qi JS, Song CP, Wang BS, Zhou JM, Kangasjarvi J, Zhu JK, Gong ZZ** (2018) Reactive oxygen species signaling and stomatal movement in plant responses to drought stress and pathogen attack. *J Integr Plant Biol* **60**: 805–826
- Qiu QS, Guo Y, Dietrich MA, Schumaker KS, Zhu JK** (2002) Regulation of SOS1, a plasma membrane Na^+/H^+ exchanger in *Arabidopsis thaliana*, by SOS2 and SOS3. *Proc Natl Acad Sci USA* **99**: 8436–8441
- Rudashevskaya EL, Ye J, Jensen ON, Fuglsang AT, Palmgren MG** (2012) Phosphosite mapping of P-type plasma membrane H^+ -ATPase in homologous and heterologous environments. *J Biol Chem* **287**: 4904–4913
- Schroeder JI, Allen GJ, Hugouvieux V, Kwak JM, Waner D** (2001) Guard cell signal transduction. *Annu Rev Plant Physiol Plant Mol Biol* **52**: 627–658
- Schroeder JI, Hagiwara S** (1990) Repetitive increases in cytosolic Ca^{2+} of guard cells by abscisic acid activation of nonselective Ca^{2+} permeable channels. *Proc Natl Acad Sci USA* **87**: 9305–9309
- Shang Y, Dai C, Lee MM, Kwak JM, Nam KH** (2016) BRI1-associated receptor kinase 1 regulates guard cell ABA signaling mediated by open stomata 1 in Arabidopsis. *Mol Plant* **9**: 447–460
- Shimazaki K, Doi M, Assmann SM, Kinoshita T** (2007) Light regulation of stomatal movement. *Annu Rev Plant Biol* **58**: 219–247
- Shimazaki K, Iino M, Zeiger E** (1986) Blue light-dependent proton extrusion by guard-cell protoplasts of *Vicia faba*. *Nature* **319**: 324–326
- Sirichandra C, Gu D, Hu HC, Davanture M, Lee S, Djaoui M, Valot B, Zivy M, Leung J, Merlot S, et al** (2009) Phosphorylation of the Arabidopsis AtrbohF NADPH oxidase by OST1 protein kinase. *FEBS Lett* **583**: 2982–2986
- Soma F, Takahashi F, Suzuki T, Shinozaki K, Yamaguchi-Shinozaki K** (2020) Plant Raf-like kinases regulate the mRNA population upstream of ABA-unresponsive SnRK2 kinases under drought stress. *Nat Commun* **11**: 1373
- Sondergaard TE, Schulz A, Palmgren MG** (2004) Energization of transport processes in plants. Roles of the plasma membrane H^+ -ATPase. *Plant Physiol* **136**: 2475–2482
- Suhita D, Raghavendra AS, Kwak JM, Vavasseur A** (2004) Cytoplasmic alkalization precedes reactive oxygen species production during methyl jasmonate- and abscisic acid-induced stomatal closure. *Plant Physiol* **134**: 1536–1545
- Svennelid F, Olsson A, Piotrowski M, Rosenquist M, Ottman C, Larsson C, Oecking C, Sommarin M** (1999) Phosphorylation of Thr-948 at the C terminus of the plasma membrane H^+ -ATPase creates a binding site for the regulatory 14-3-3 protein. *Plant Cell* **11**: 2379–2391
- Takahashi Y, Zhang JB, Hsu PK, Ceciliato PHO, Zhang L, Dubeaux G, Munemasa S, Ge CN, Zhao YD, Hauser F, et al** (2020) MAP3Kinase-dependent SnRK2-kinase activation is required for abscisic acid signal transduction and rapid osmotic stress response. *Nat Commun* **11**: 12
- Takemiya A, Kinoshita T, Asanuma M, Shimazaki K** (2006) Protein phosphatase 1 positively regulates stomatal opening in response to blue light in *Vicia faba*. *Proc Natl Acad Sci USA* **103**: 13549–13554
- Takemiya A, Sugiyama N, Fujimoto H, Tsutsumi T, Yamauchi S, Hiyama A, Tada Y, Christie JM, Shimazaki KI** (2013) Phosphorylation of BLUS1 kinase by phototropins is a primary step in stomatal opening. *Nat Commun* **4**: 2094
- Thaminy S, Miller J, Stagljar I** (2004) The split-ubiquitin membrane-based yeast two-hybrid system. *Methods Mol Biol* **261**: 297–312
- Ueno K, Kinoshita T, Inoue S, Emi T, Shimazaki K** (2005) Biochemical characterization of plasma membrane H^+ -ATPase activation in guard cell protoplasts of *Arabidopsis thaliana* in response to blue light. *Plant Cell Physiol* **46**: 955–963
- Vahisalu T, Kollist H, Wang YF, Nishimura N, Chan WY, Valerio G, Lamminmäki A, Brosché M, Moldau H, Desikan R, et al** (2008) SLAC1 is required for plant guard cell S-type anion channel function in stomatal signalling. *Nature* **452**: 487–491
- Wang FF, Lian HL, Kang CY, Yang HQ** (2010) Phytochrome B is involved in mediating red light-induced stomatal opening in *Arabidopsis thaliana*. *Mol Plant* **3**: 246–259
- Wang WJ, Chen QB, Xu SM, Liu WC, Zhu XH, Song CP** (2020) Trehalose-6-phosphate phosphatase E modulates ABA-controlled root growth and stomatal movement in Arabidopsis. *J Integr Plant Biol* **62**: 1518–1534
- Wang XQ, Ullah H, Jones AM, Assmann SM** (2001) G protein regulation of ion channels and abscisic acid signaling in Arabidopsis guard cells. *Science* **292**: 2070–2072
- Wang Y, Kinoshita T** (2017) Measurement of stomatal conductance in rice. *Bio Protoc* **7**: e2226
- Wegner LH, Shabala S** (2020) Biochemical pH clamp: the forgotten resource in membrane bioenergetics. *New Phytol* **225**: 37–47
- Wegner LH, Li XW, Zhang J, Yu M, Shabala S, Hao ZF** (2021) Biochemical and biophysical pH clamp controlling Net H^+ efflux across the plasma membrane of plant cells. *New Phytol* **230**: 408–415

- Wei ZY, Li J** (2018) Receptor-like protein kinases: key regulators controlling root hair development in *Arabidopsis thaliana*. *J Integr Plant Biol* **60**: 841–850
- Wu D, Liu YA, Xu F, Zhang YL** (2018) Differential requirement of BAK1 C-terminal tail in development and immunity. *J Integr Plant Biol* **60**: 270–275
- Wu QQ, Wang M, Shen JL, Chen DH, Zheng Y, Zhang W** (2019) ZmOST1 mediates abscisic acid regulation of guard cell ion channels and drought stress responses. *J Integr Plant Biol* **61**: 478–491
- Xue J, Gong BQ, Yao XR, Huang XJ, Li JF** (2020) BAK1-mediated phosphorylation of canonical G protein alpha during flagellin signaling in *Arabidopsis*. *J Integr Plant Biol* **62**: 690–701
- Xue Y, Yang Y, Yang Z, Wang X, Guo Y** (2018) VAMP711 is required for abscisic acid-mediated inhibition of plasma membrane H⁺-ATPase activity. *Plant Physiol* **178**: 1332–1343
- Yan S, McLamore ES, Dong S, Gao H, Taguchi M, Wang N, Zhang T, Su X, Shen Y** (2015) The role of plasma membrane H⁺-ATPase in jasmonate-induced ion fluxes and stomatal closure in *Arabidopsis thaliana*. *Plant J* **83**: 638–649
- Yang L, Zhang J, He JN, Qin YY, Hua DP, Duan Y, Chen ZZ, Gong ZZ** (2014) ABA-mediated ROS in mitochondria regulate root meristem activity by controlling PLETHORA expression in *Arabidopsis*. *PLoS Genet* **10**: e1004791
- Yang Y, Qin Y, Xie C, Zhao F, Zhao J, Liu D, Chen S, Fuglsang AT, Palmgren MG, Schumaker KS, et al** (2010) The *Arabidopsis* chaperone J3 regulates the plasma membrane H⁺-ATPase through interaction with the PKS5 kinase. *Plant Cell* **22**: 1313–1332
- Yang YQ, Wu YJ, Ma L, Yang ZJ, Dong QY, Li QP, Ni XP, Kudla J, Song CP, Guo Y** (2019) The Ca²⁺ sensor SCaBP3/CBL7 modulates plasma membrane H⁺-ATPase activity and promotes alkali tolerance in *Arabidopsis*. *Plant Cell* **31**: 1367–1384
- Yin Y, Adachi Y, Ye WX, Hayashi M, Nakamura Y, Kinoshita T, Mori IC, Murata Y** (2013) Difference in abscisic acid perception mechanisms between closure induction and opening inhibition of stomata. *Plant Physiol* **163**: 600–610
- Zhang S, Li C, Ren H, Zhao T, Li Q, Wang S, Zhang Y, Xiao F, Wang X** (2020) BAK1 Mediates light intensity to phosphorylate and activate catalases to regulate plant growth and development. *Inter J Mol Sci* **21**: 1437
- Zhang X, Dong FC, Gao JF, Song CP** (2001) Hydrogen peroxide-induced changes in intracellular pH of guard cells precede stomatal closure. *Cell Res* **11**: 37–43
- Zhang X, Wang H, Takemiya A, Song CP, Kinoshita T, Shimazaki K** (2004) Inhibition of blue light-dependent H⁺ pumping by abscisic acid through hydrogen peroxide-induced dephosphorylation of the plasma membrane H⁺-ATPase in guard cell protoplasts. *Plant Physiol* **136**: 4150–4158
- Zhou Q, Liu J, Wang JY, Chen SF, Chen LJ, Wang JF, Wang HB, Liu B** (2020) The juxtamembrane domains of *Arabidopsis* CERK1, BAK1, and FLS2 play a conserved role in chitin-induced signaling. *J Integr Plant Biol* **62**: 556–562
- Zhu YJ, Hu XY, Duan Y, Li SF, Wang Y, Rehman AU, He JN, Zhang J, Hua DP, Yang L, et al** (2020) The *Arabidopsis* nodulin homeobox factor AtNDX interacts with AtRING1A/B and negatively regulates abscisic acid signaling. *Plant Cell* **32**: 703–721